PTEP

Prog. Theor. Exp. Phys. **2012**, 01A204 (36 pages)
DOI: 10.1093/ptep/pts015

Gaussian expansion method for few-body systems and its applications to atomic and nuclear physics

Emiko Hiyama

Nishina Center for Accelerator-Based Science, RIKEN, Wako, Saitama 351-1098, Japan
E-mail: hiyama@riken.jp

Received April 13, 2012; Accepted July 3, 2012; Published September 14, 2012

The Gaussian expansion method and its application to various three-, four-, and five-body problems are reviewed. As examples for the application, we review i) the application to three- and four-body ^{4}He-atom clusters and ii) benchmark testing for four-nucleon bound states using realistic force and calculation of the second 0^+ state of ^{4}He, iii) the four-body calculation of ${}^{4}_{\Lambda}$H and ${}^{4}_{\Lambda}$He taking ΛN–ΣN coupling, and iv) the five-body calculation of a double Λ hypernucleus, ${}^{11}_{\Lambda}$Be. In addition, we discuss the understanding of the structure and the mechanisms of those systems together with some useful techniques for the calculations. We obtain the first numerically reliable solution to the binding energies and wave functions of the four-body system of ^{4}He atoms interacting with an extremely strong short-range repulsion and a weak van der Waals attraction. By applying the method to the calculations of the four-nucleon bound state, we find that the drastic change in the spatial structure between the 0^+_1 to 0^+_2 states is well understood in terms of the GEM four-body calculation. The four-body calculations are performed for ${}^{4}_{\Lambda}$H and ${}^{4}_{\Lambda}$He and the role of Λ–Σ conversion in these hypernuclei is discussed. Energy levels of the double Λ hypernucleus, ${}^{11}_{\Lambda\Lambda}$Be, are calculated within the framework of an $\alpha\alpha n\Lambda\Lambda$ five-body model. The Hida event, recently observed in the KEK-E373 experiment, is interpreted as an observation of the ground state of ${}^{11}_{\Lambda\Lambda}$Be.

1. Introduction

Many important problems in physics can be addressed by solving, with high precision, Schrödinger equations for few-body systems. For the study of such problems where accurate calculations are required, the Gaussian expansion method (GEM), an ab initio variational method for few-body systems, was proposed by Kamimura [1,2] some 24 years ago to carry out nonadiabatic three-body calculations of muonic molecules and muon–atomic collisions. These systems are very good testing grounds for atomic and molecular models and few-body calculations, since there are more observable quantities than in analogous electron systems because of the large muon mass. The structure of the muonic molecule $(dt\mu)_J$ and the muon transfer reaction $(d\mu)_{1s} + t \rightarrow (t\mu)_{1s} + d$ are of particular interest since they are the key to muon-catalyzed fusion (μCF) (e.g. Ref. [3]). An accuracy of up to seven significant figures in the calculated three-body binding energy and an accurate wave function in the tail region were required for the very weakly bound excited $J = 1$ state. The calculation using GEM satisfied this.

Since the muon mass is 207 times the electron mass, nonadiabatic treatment of the three charged particles is necessary. This difficulty, as well as the practical interest in the energy production by μCF, has stimulated studies into the problems by means of various methods in nuclear physics,

© The Author(s) 2012. Published by Oxford University Press on behalf of the Physical Society of Japan.
This is an Open Access article distributed under the terms of the Creative Commons Attribution License (http://creativecommons.org/licenses/by/3.0), which permits unrestricted use, distribution, and reproduction in any medium, provided the original work is properly cited.

Downloaded from https://academic.oup.com/ptep/article/2012/1/01A204/1565231 by University of Manchester user on 22 August 2022

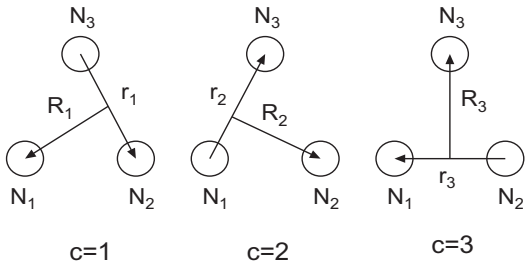

Fig. 1. Three Jacobian coordinates of a three-body system.

atomic/molecular physics and quantum chemistry. Among these methods, GEM has made one of the best contributions to a variety of three-body scattering and bound-state problems appearing in μCF.

The characteristics of GEM are as follows, in the case of the solution to three-body bound states by diagonalizing the Hamiltonian in a space spanned by a finite number of L^2 three-body basis functions:

(i) The three-body basis set consists of functions of Jacobian coordinates $(\mathbf{r}_c, \mathbf{R}_c)$ of *all* three rearrangement channels ($c = 1, 2, 3$) shown in Fig. 1, each base being in the form $\phi_{n_c l_c}(r_c)\psi_{N_c L_c}(R_c)\,[Y_{l_c}(\hat{\mathbf{r}}_c)\,Y_{L_c}(\hat{\mathbf{R}}_c)]_{JM}$ with obvious notations for angular momenta, n_c and N_c specifying the radial dependence.

(ii) The radial dependence is Gaussian, $\phi_{nl}(r) = r^l\, e^{-\nu_n r^2}$, with the range parameters forming a geometric progression $\{\nu_n = \nu_1 a^{n-1}; n = 1, \ldots, n_{\max}\}$ and similarly for $\psi_{NL}(R)$.

We remark that a single Gaussian decays quickly as r increases, but appropriate superposition of many Gaussians can decay even exponentially up to a sufficiently large distance, as demonstrated later. The preparation of the basis functions in all three channels makes the function space significantly larger (even if l and L are strongly restricted) than the case using the basis functions of a single channel alone but makes the nonorthogonality between the basis functions much less troublesome than in the latter case. These types of three-channel basis functions are particularly suitable for describing both short-range correlations and long-range tail behavior in the asymptotic region of few-body wave functions. The Gaussian shape of the basis functions makes the calculation of the Hamiltonian matrix elements easy even between basis functions of different channels.

Prescriptions (i) and (ii) are the main reasons for the success of GEM in various types of three-body bound and quasi-bound states such as muonic molecules [1,2,4–7], three-nucleon bound states (^{3}H, ^{3}He) [8,9], weakly bound states in unstable nuclei [10–13], and antiprotonic helium atoms [14–17] (theoretical contribution to the first determination of the antiproton mass in Particle Listings 2000 [18]).

When one proceeds to four-body systems, calculation of the Hamiltonian matrix elements becomes much more laborious. In order to make the four-body calculation tractable even for complicated interactions, the present author has proposed the infinitesimally-shifted Gaussian lobe basis functions [19,20], which are precisely presented in the GEM review paper [21]. The Gaussian basis function $r^l e^{-\nu_n r^2} Y_{lm}(\hat{\mathbf{r}})$ is replaced, mathematically equivalently, by a superposition of infinitesimally-shifted Gaussians, $\lim_{\varepsilon\to 0} \frac{1}{(\varepsilon\nu_n)^l} \sum_{k=1}^{k_{\max}} C_{lm,k}\, e^{-\nu_n(\mathbf{r} - \varepsilon\mathbf{D}_{lm,k})^2}$, whose parameters $\{C_{lm,k}, \mathbf{D}_{lm,k};\ k = 1, \ldots, k_{\max}\}$ are so determined that the latter is equivalent to the former. We make a similar replacement for the basis functions of all the other Jacobian coordinates. Thanks to the absence of spherical harmonics, use of the latter functional forms makes the matrix element calculation extremely easy in practice, with no tedious angular-momentum algebra.

Downloaded from https://academic.oup.com/ptep/article/2012/1/01A204/1565231 by University of Manchester user on 22 August 2022

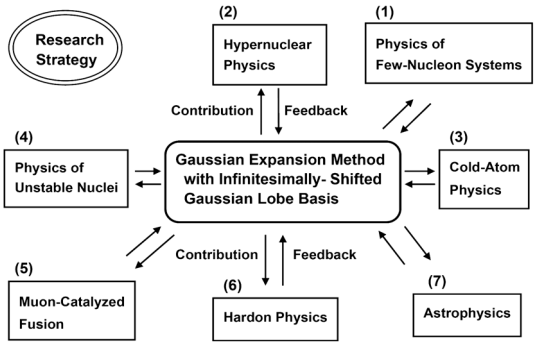

Fig. 2. Strategy of our research using GEM.

The GEM with the technique of infinitesimally-shifted Gaussians [19–21] has been applied to various three-, four-, and five-body calculations in hypernuclei [22–28], the four-nucleon system [29, 30], μCF in double-muonic molecules [31], the penta-quark system [32], stau-catalyzed big-bang nucleosynthesis [33], and ultracold-atom systems [34–36].

We have been studying many subjects in various research fields of physics using the more developed GEM. The strategy for such studies is as follows. As shown in Fig. 2, we have our own calculation method GEM in the center of the strategy. We have been applying the GEM to various research fields, such as (1) the physics of few-nucleon systems, (2) hypernuclear physics, (3) ultracold-atom physics, (4) the physics of unstable nuclei, (5) muon-catalyzed fusion, (6) hadron physics, and (7) astrophysics, and have contributed to the development of each research field. As a feedback of the numerical efforts for the contributions, we have been able to develop further the calculation method GEM at the center, and then apply the developed GEM to the new field which author has never researched. We have been repeating this type of research cycle under this strategy.

The purpose of the present review paper is to discuss some successful examples of the application of GEM to (1) the physics of few-nucleon systems, (2) hypernuclear physics, and (3) ultracold-atom physics, together with brief survey of the calculation procedure of GEM.

(1) Few-nucleon systems Calculation of the four-nucleon ground state, ^{4}He(0^+_1), using a realistic force is useful for testing various calculation methods and schemes for few-body systems. Eighteen authors from different research groups, including the present author, performed a benchmark test calculation in Ref. [29]. They demonstrated that the Schrödinger equation for the four-nucleon ground state can be handled quite reliably by different methods, leading to very good agreement in the binding energy, expectation values of the kinetic and potential energies, and simple wave function properties. The next challenge is to apply the methods to the second 0^+ state of ^{4}He, which has the same spin, isospin, and parity as the ground state and therefore should have quite different spatial structure in order to be orthogonal to the 0^+_1 state. By applying GEM to this subject, the present author and collaborators [30] succeeded, for the first time, in describing both the compact bound state (0^+_1) and very dilute excited state (0^+_2) simultaneously, together with the transition between them, by explaining the observed form factor of ^{4}He$(e, e')^4$He(0^+_2).

(2) Hypernuclei GEM has been most extensively applied to the study of hypernuclear physics by the present author and collaborators. The calculations and results are presented in the review papers [21,37–40].

The hyperon (Y)–nucleon (N) and hyperon (Y)–hyperon (Y) interactions proposed so far exhibit a great deal of ambiguity, since YN scattering experiments are extremely limited, and there are no YY

Downloaded from https://academic.oup.com/ptep/article/2012/1/01A204/1565231 by University of Manchester user on 22 August 2022

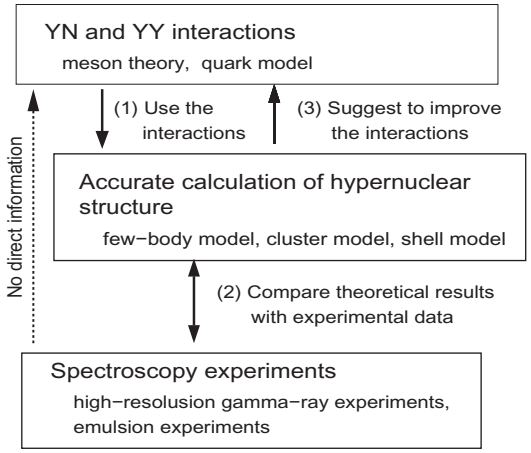

Fig. 3. Strategy for extracting information about YN and YY interactions from the study of the structure of light hypernuclei.

scattering data. One can, however, obtain useful information on the YN and YY interaction combining few-body calculations of the hypernuclear structure and the related spectroscopy experiments on the basis of the following strategy (Fig. 3):

(i) Firstly, we begin with candidates of YN and YY interactions that are based on the meson theory and/or the constituent quark model.
(ii) We then utilize spectroscopy experiments of hypernuclei. Generally, the experiments do not *directly* give any information about the YN and YY interactions.
(iii) Using the interactions in (i), accurate calculations of hypernuclear structures are performed. The calculated results are compared with the experimental data.
(iv) On the basis of this comparison, improvements for the underlying interaction models are proposed.

Following this strategy, we succeeded in extracting information on the YN and YY interactions proposed so far with full use of GEM. As a typical example, we review the structure of ${}^{4}_{\Lambda}$H, ${}^{4}_{\Lambda}$He, and the double Λ hypernucleus, ${}^{11}_{\Lambda\Lambda}$Be.

One of the important subject in hypernuclear physics is to calculate few-body systems taking account of particle conversion such as ΛN–ΣN. For this purpose, hypernuclear physics provides us with many interesting subjects to develop our GEM. As an example, in Ref. [26], the present author and collaborators performed, for the first time, an explicit four-body calculation of ${}^{4}_{\Lambda}$H and ${}^{4}_{\Lambda}$He taking the $\Lambda N - \Sigma N$ coupling explicitly between the $NNN\Lambda$ and $NNN\Sigma$ channels. This enabled them to precisely analyze the role of the $\Lambda N - \Sigma N$ coupling in those hypernuclei which had for a long time been the subject of investigations by various authors [41–43] to see the effect of the conversion on the binding energies, the charge-symmetry breaking effect, the role of the ΛNN three-body force, etc.

New observation of a double-Λ hypernucleus, called the Hida event [44]. provided us with an opportunity to develop our method to the five-body problem. This event has two possible interpretations: One is ${}^{11}_{\Lambda\Lambda}$Be with $B_{\Lambda\Lambda} = 20.83 \pm 1.27$ MeV and the other is ${}^{12}_{\Lambda\Lambda}$Be with $B_{\Lambda\Lambda} = 22.48 \pm 1.21$ MeV. It is uncertain whether this is an observation of a ground state or an excited state. In Ref. [45], the present author and collaborators studied the possibility of ${}^{11}_{\Lambda\Lambda}$Be employing the $\alpha\alpha n\Lambda\Lambda$

Downloaded from https://academic.oup.com/ptep/article/2012/1/01A204/1565231 by University of Manchester user on 22 August 2022

five-body cluster model. This five-body cluster model is quite pioneering as a numerical computation, since there exist three species of particle, α, Λ, and n; five kinds of interactions (Λ–Λ, Λ–n, Λ–α, α–n, and α–α) are involved, and one must take into account the Pauli principle between the two α particles and between the α and n. It should be emphasized, before going to the five-body calculation, that the following conditions should be satisfied: All the interactions are determined so as to reproduce the observed binding energies of the two- and three-body subsystems ($\alpha\alpha$, αn, $\alpha\alpha n$, $\alpha\Lambda$, $\alpha\alpha\Lambda$, $\alpha\Lambda\Lambda$, and $\alpha n\Lambda$). Then, the calculated binding energies of the $A = 10$ four-body subsystems, ${}^{10}_{\Lambda}$Be ($= \alpha\alpha n\Lambda$) and ${}^{10}_{\Lambda\Lambda}$Be ($= \alpha\alpha\Lambda\Lambda$), should reproduce the observed values with no additional parameter. It was possible to set the above interactions so as to satisfy these severe constraints. We were then able to calculate both the ground and excited states of ${}^{11}_{\Lambda\Lambda}$Be with no free parameter. On the basis of careful calculations, we showed in Ref. [45] that the Hida event can be interpreted as the observation of the ground state of ${}^{11}_{\Lambda\Lambda}$Be.

(3) Ultracold atoms Recently, the present author and collaborators [34–36] applied GEM to an important fundamental problem in ultracold-atom physics; namely, we obtained the first numerically reliable solution to the binding energies and wave functions of the four-body systems (tetramer) of ^{4}He atoms, which are very weakly bound states interacting with an extremely strong short-range repulsion and a weak van der Waals attraction. We found that precisely the same shape of the short-range correlation as seen in the ^{4}He dimer appears in the ^{4}He trimer and tetramer ground and excited states; this gives a foundation to the a priori assumption that a two-particle correlation function (such as the Jastrow function) to simulate the short-range part of the two-body radial wave function is incorporated in the three- and four-body wave functions from the beginning. From analysis of the accurately obtained asymptotic behavior of the ^{4}He two- to four-body wave functions, we proposed the dimerlike-pair model. This model suggests that the binding energy of the excited state of N-atom clusters can be represented as $\frac{B_N^{(2)}}{B_2} = \frac{B_{N-1}^{(1)}}{B_2} + \frac{N}{2(N-1)}$. Here, $B_N^{(1)}$ and $B_N^{(2)}$ denote the binding energy of the ground state and the first excited state of N^4He-atom clusters. This relation was found in Ref. [34] and must be the simplest (but accurate) universal property of weakly bound cluster systems. We also found that the binding energies of the trimer and tetramer ground and excited states exhibit perfect linear correlations (generalized Tjon lines).

This paper is organized as follows. In Sect. 2, we briefy explain GEM in two-body systems and test it in various situations of the systems. In Sect. 3, we briefly explain GEM in three- and four-body systems, show an application to the trimer and tetramer of ^{4}He-atom clusters, and discuss a universality in atomic and nuclear physics. Emphasis is placed on the precise solution to the Schrödinger equations for weakly bound states of three (four) particles that are interacting with a very strong short-range repulsive core. In Sect. 4, we present a precise four-nucleon GEM calculation for the ground and first excited 0^+ states of ^{4}He and the transition between them. In Sect. 5, we demonstrate the successful application of GEM to the study of four-body and five-body structure of light hypernuclei. A summary is given in Sect. 6.

2. Gaussian basis functions for few-body systems

2.1. Rayleigh–Ritz variational method

We consider how to solve the Schrödinger equation for bound states of a few-body system with the total angular momentum J and the z-component M

$$(H - E)\Psi_{JM} = 0 \tag{2.1}$$

Downloaded from https://academic.oup.com/ptep/article/2012/1/01A204/1565231 by University of Manchester user on 22 August 2022

using the Rayleigh–Ritz variational method. The other quantum numbers such as parity and isospin are omitted for simplicity. We expand the total wave function in terms of a set of L^2-integrable basis functions $\{\Phi_{JM,n}; n = 1, \ldots, n_{\max}\}$ as

$$\Psi_{JM} = \sum_{n=1}^{n_{\max}} C_n^{(J)} \Phi_{JM,n}. \tag{2.2}$$

The eigenenergy and the coefficients $C_n^{(J)}$ are obtained by

$$\langle \Phi_{JM,n} | H - E | \Psi_{JM} \rangle = 0, \qquad (n = 1, \ldots, n_{\max}), \tag{2.3}$$

which leads to a generalized matrix eigenvalue problem

$$\sum_{n'=1}^{n_{\max}} (H_{nn'}^{(J)} - E N_{nn'}^{(J)}) C_{n'}^{(J)} = 0, \qquad (n = 1, \ldots, n_{\max}), \tag{2.4}$$

where the energy and overlap matrix elements are given by

$$H_{nn'}^{(J)} = \langle \Phi_{JM,n} | H | \Phi_{JM,n'} \rangle, \tag{2.5}$$

$$N_{nn'}^{(J)} = \langle \Phi_{JM,n} | 1 | \Phi_{JM,n'} \rangle. \tag{2.6}$$

By solving the eigenvalue problem, we can obtain not only the lowest state but also the excited-state eigenfunctions with the same J and parity.

An important issue of the variational method is how to select a good set of basis functions $\{\Phi_{JM,n}; n = 1, \ldots, n_{\max}\}$. There are many candidates for two-body systems, but, for systems with more than two bodies, construction of a good set of basis functions is not easy, and calculation of the matrix elements (2.5) and (2.6) becomes very laborious. From this point of view, real-range Gaussians (see Sect. 2.2) and complex-range Gaussians (see Sect. 2.3) written using all the possible sets of Jacobi coordinates are particularly suitable, not only for the calculation of the matrix elements but also for the description of the short-range correlations, long-range tail behavior, and highly oscillatory character of few-body wave functions.

It is to be emphasized that, in the GEM few-body calculations, proper short-range correlation and asymptotic behavior of the total wave function are *automatically* obtained by solving the Schrödinger equation (2.2) using the above basis functions for ab initio calculations.

In this section, we shall show good examples to demonstrate the usefulness of the real- and complex-range Gaussian basis functions for describing i) one-body Woods–Saxon shell-model states, ii) highly (excited) oscillating states, and iii) very weakly bound states in the presence of a strong short-range repulsion.

2.2. *Gaussian basis set with ranges in geometric progression*

Let us consider the one- or two-body Schrödinger equation

$$[-\hbar^2/(2\mu)\nabla^2 + V(r) - E]\Psi_l(r)Y_{lm}(\hat{\mathbf{r}}) = 0, \tag{2.7}$$

where μ is the reduced mass and $V(r)$ is a central potential. $\Psi(r)Y_{lm}(\hat{\mathbf{r}})$ is the wave function with angular momentum l and its z-component m. The GEM recommends expanding $\psi_l(r)$ in terms of a

Downloaded from https://academic.oup.com/ptep/article/2012/1/01A204/1565231 by University of Manchester user on 22 August 2022

Table 1. Binding energies of the $0s$, $1s$, and $0d$ states of a neutron in the Woods–Saxon potential (see text) by exact and GEM calculations. The Gaussian basis set is $\{n_{\max} = 8, r_1 = 1.0\,\text{fm}, r_{\max} = 6.0\,\text{fm}\}$.

	Exact	GEM ($n_{\max} = 8$)
E_{0s} (MeV)	-33.2531	-33.2528
E_{1s} (MeV)	-3.2221	-3.2208
E_{0d} (MeV)	-2.1897	-2.1893

set of Gaussian basis functions, $\phi_{nl}(r)$, whose ranges are set in a *geometric* progression:

$$\Psi_l(r) = \sum_{n=1}^{n_{\max}} c_{nl}\,\phi_{nl}(r), \tag{2.8}$$

$$\phi_{nl}(r) = r^l\, e^{-\nu_n r^2}, \tag{2.9}$$

$$\nu_n = \frac{1}{r_n^2}, \quad r_n = r_1\, a^{n-1} \qquad (n = 1, \ldots, n_{\max}). \tag{2.10}$$

The normalization constant in Eq. (2.9) is omitted for simplicity. The basis functions $\{\phi_{nl}\}$ have the following properties:

i) They can range from very compact to very diffuse, more densely in the inner region than in the outer one. While the bases with small ranges are responsible for describing the short-range structure of the system, the bases with the longest-range parameters are for asymptotic behavior.

ii) They, multiplied by normalization constants for $\langle \phi_{nl} \mid \phi_{nl} \rangle = 1$, have a relation

$$\langle \phi_{n\,l} \mid \phi_{n+k\,l} \rangle = [2a^k/(1 + a^{2k})]^{l+3/2}, \tag{2.11}$$

which shows that the overlap with the kth neighbor is *independent* of n, decreasing gradually with increasing k.

We then expect that coupling between all the basis functions takes place smoothly and coherently so as to describe properly both the short-range structure and long-range asymptotic behavior simultaneously. We note that a single Gaussian decays quickly as r increases, but appropriate superposition of many Gaussians can decay even exponentially up to a sufficiently large distance.

The setting of the Gaussian ranges, Eq. (2.10), greatly reduces the number of nonlinear parameters to be optimized. We designate a set of the geometric sequence by $\{n_{\max}, r_1, r_{n_{\max}}\}$ instead of $\{n_{\max}, r_1, a\}$, which is more convenient for consideration of the spatial distribution of the basis set. Optimization of the nonlinear range parameters is in principle by a trial and error procedure but a great deal of experience and systematics have been accumulated in many studies using the GEM.

We present an instructive example of the application of GEM to a potential problem that one often meets in e.g. the Woods–Saxon shell model and nucleon-transfer reactions; namely, calculation of nucleon bound states in a Woods–Saxon potential:

$$V(r) = V_0/[1 + \mathrm{e}^{(r-R_0)/a}]. \tag{2.12}$$

Here, we take the case of $V_0 = -55\,\text{MeV}$, $R_0 = 3.0\,\text{fm}$, $a = 0.6\,\text{fm}$, and $\mu = m$ with $\hbar^2/m = 41.47\,\text{MeV}$, and solve the $0s$, $1s$, and $0d$ states.

The energy values obtained by the exact calculation are listed in Table 1. We solved Eq. (2.7) taking a Gaussian basis set $\{n_{\max} = 8, r_1 = 1.0\,\text{fm}, r_{n_{\max}} = 6.0\,\text{fm}\}$. We find, in Table 1, that sufficiently

Downloaded from https://academic.oup.com/ptep/article/2012/1/01A204/1565231 by University of Manchester user on 22 August 2022

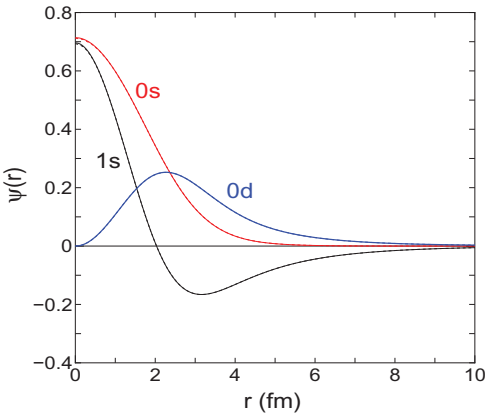

Fig. 4. Wave functions of the $0s$, $1s$, and $0d$ states of a nucleon in a Woods–Saxon potential (2.12). The solid curve denotes the GEM result with eight Gaussians, whereas the dotted curve is the exact one (both curves almost overlap in the whole region).

accurate results are obtained by GEM. In Fig. 4, the wave functions given by the eight Gaussian basis functions are almost the same as those given by the exact calculation.

We recommend the use of the above types of Gaussian basis functions to represent the eigenfunctions of the Woods–Saxon shell model. Calculation of interaction matrix elements that need coordinate transformations will become easy.

2.3. *Complex-range Gaussian basis functions*

Although the Gaussian basis functions are suitable for representing short-range correlations and long-range tail behavior, it is difficult to reproduce highly oscillatory functions with more than ∼5 nodes with good accuracy. Such oscillating functions can appear e.g. when treating highly excited vibrational states and when discretizing the continuum states [12]. Also, such functions are necessary to describe the amplitude of a scattering state in the interaction region if one utilizes the Kohn-type variational method (see Refs. [33,46] and Sect. 2.5 of Ref. [21]).

Although the eigenfunctions for a harmonic oscillator potential have highly oscillatory members, they are not useful for three- and more-body systems because calculation of the matrix elements with them is very hard when the coordinate transformations are needed in the integration. One needs good basis functions with highly oscillatory members that are easy to use for few-body calculations.

GEM recommends [21] useful basis functions that satisfy the above requirements. They are Gaussian functions multiplied by *cosine* and *sine* functions of r^2:

$$\phi_{nl}^{(\cos)}(r) = r^l\, e^{-\nu_n r^2} \cos\omega\nu_n r^2 = r^l \frac{e^{-\eta_n^* r^2} + e^{-\eta_n r^2}}{2},\ (n = 1, \ldots, n_{\max}) \tag{2.13}$$

$$\phi_{nl}^{(\sin)}(r) = r^l\, e^{-\nu_n r^2} \sin\omega\nu_n r^2 = r^l \frac{e^{-\eta_n^* r^2} - e^{-\eta_n r^2}}{2i},\ (n = 1, \ldots, n_{\max}), \tag{2.14}$$

where $\eta_n = (1 + i\,\omega)\,\nu_n$ and $\eta_n^* = (1 - i\,\omega)\,\nu_n$. Normalization is omitted for simplicity. The Gaussian sizes $\nu_n (= 1/r_n^2)$ are taken to form a geometric progression in the same manner as in Eq. (2.10). The parameter ω is a free parameter in principle, but numerical tests suggest taking $\omega \sim 1$. The new bases apparently extend the function space from the old ones (2.9) since they have oscillating components.

Downloaded from https://academic.oup.com/ptep/article/2012/1/01A204/1565231 by University of Manchester user on 22 August 2022

Table 2. Test of the accuracy of real-range Gaussian and complex-range Gaussian basis functions for highly excited states ($l = 0, n \leq 22$) of a harmonic oscillator potential. The number of basis functions is 28 for both cases. Energies are listed in terms of the number of quanta, $E/\hbar\omega - \frac{3}{2}$.

Exact	Gaussian	Complex-range	Exact	Gaussian	Complex-range
0.0	0.0000	0.0000	24.0	24.1	24.0001
4.0	4.0000	4.0000	28.0	29.5	28.0003
8.0	8.0000	8.0000	32.0	37.3	32.002
12.0	12.0000	12.0000	**38.0**	53.8	**38.003**
16.0	16.002	16.0000	42.0	69.9	42.1
20.0	20.01	20.0000	46.0	91.6	46.3

We simply refer to the functions (2.13) and (2.14) as 'complex-range Gaussians' although they are Gaussians multiplyed by *cosine* (*sine*) function of r^2, whereas we call the functions on the RHS of Eq. (2.9) 'real-range Gaussians' when necessary.

The reason why the functions $\phi_{nl}^{(\cos)}(r)$ and $\phi_{nl}^{(\sin)}(r)$ are easy to use in numerical calculations is as follows. Since they can be rewritten as in the RHS of the second equality in Eqs. (2.13) and (2.14), calculation of the matrix elements can be done using essentially the same computer program for real-range Gaussians with some real variables replaced by complex ones. This is an advantage of adopting complex-range Gaussians. Note that with complex-range Gaussian basis functions, the total number of basis functions is $2n_{\max}$.

A good test of the use of complex-range Gaussian basis functions is to calculate the wave functions of highly excited states in a harmonic oscillator potential. We take the case of a nucleon with angular momentum $l = 0$ in a potential having $\hbar\omega = 15.0$ MeV. We expand the s-state wave function, Ψ_0, as

$$\Psi_0(r) = \sum_{n=1}^{n_{\max}} \left[c_n^{(\cos)} \phi_{n0}^{(\cos)}(r) + c_n^{(\sin)} \phi_{n0}^{(\sin)}(r) \right]. \tag{2.15}$$

The parameters of the complex-range Gaussians are $\{2n_{\max} = 28, r_1 = 1.4\,\text{fm}, r_{n_{\max}} = 5.8\,\text{fm}, \omega = 1.09\}$. For the sake of comparison, we also tested the Gaussian basis functions with the parameters $\{n_{\max} = 28,\ r_1 = 0.5\,\text{fm},\ r_{n_{\max}} = 11.3\,\text{fm}\}$. The optimized r_1 and $r_{n_{\max}}$ values are quite different between the two types of bases though the total numbers of basis functions are the same. In Table 2, we compare the calculated energy eigenvalues with the exact ones. It is evident that the complex-range Gaussians can reproduce up to much more highly excited states than the real-range Gausssians do.

Figure 5 demonstrates the high accuracy of the wave function of the 19th excited state with 38 quanta. The error is within a few %, much smaller than the thickness of the line. The figure suggests that the basis function is also suitable for describing scattering wave functions in a finite space.

Another good example of the application of the complex-range Gaussian basis function is to the solution of a very weakly bound state in the presence of an extremely strong short-range repulsive core potential. Namely, we solved the Schrödiger equation for the dimer of the ^{4}He atom, which is known to have the shallowest bound ground states in nature. This solution forms the foundation of the study in Sect. 3.

One of the realistic ^{4}He–^{4}He potentials, called LM2M2 [47], is illustrated in Fig. 6 with the dotted (red) line with an extremely strong repulsive core. In Eq. (2.15), we expand Ψ_0 using 100 basis functions with a parameter set $\{n_{\max} = 50,\ r_1 = 0.5\,\text{Å},\ r_{n_{\max}} = 600.0\,\text{Å},\ \omega = 1.0\}$. We obtain $B_2 = 1.303\,48\,\text{mK}$, $\sqrt{\langle r^2 \rangle} = 70.93\,\text{Å}$, and $\langle r \rangle = 52.00$ Å which are the same as those obtained in the literature [47]. Experimentally, $\langle r \rangle = 52 \pm 4$ Å and $B_2 = 1.1^{+0.3}_{-0.2}$ mK were obtained [48].

Downloaded from https://academic.oup.com/ptep/article/2012/1/01A204/1565231 by University of Manchester user on 22 August 2022

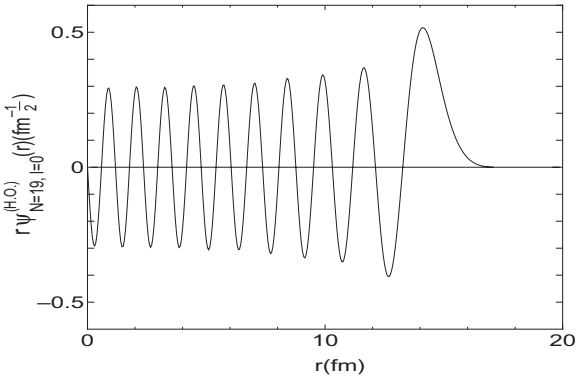

Fig. 5. Wave function of the $l = 0$, 19 ($N = 2n + l = 38$-quanta) state obtained by diagonalizing the harmonic-oscillator-potential Hamiltonian using 28 complex-range Gaussian basis functions. It is compared with the exact wave function but the difference is invisible since the error is less than a few % everywhere. See text for the Gaussian parameters.

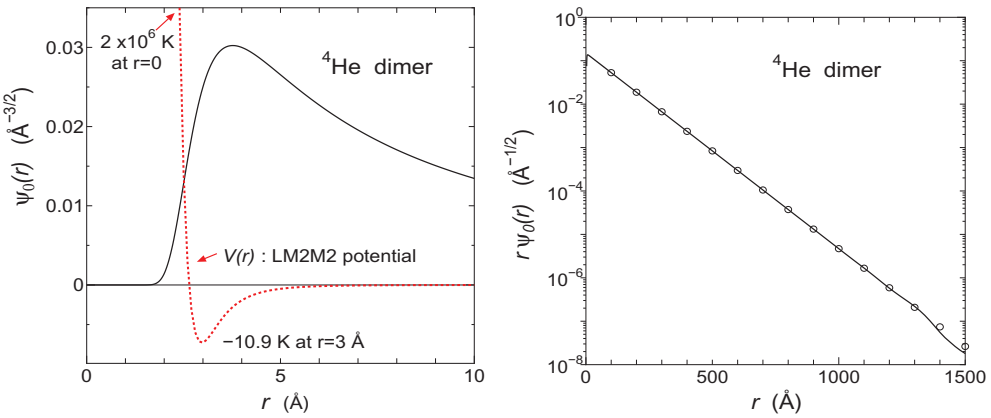

Fig. 6. Short-range structure (left) and asymptotic behavior (right) of the radial wave function $\Psi_0(r)$ of the ^{4}He dimer obtained by using the complex-range Gaussian basis functions (2.13) and (2.14). The open circles stands for the exact asymptotic form. The dotted (red) line (left) illustrates the LM2M2 potential in arbitrary units. This figure is taken from Ref. [34].

As shown in Fig. 6, both the strong short-range correlation ($x \lesssim 4$ Å) and the asymptotic behavior of the dimer are well described. $r\,\Psi_0(r)$ precisely reproduces the exact asymptotic shape $0.1498\exp(-\kappa_2 r)$ (Å$^{-1/2}$) with $\kappa_2 = \sqrt{m B_2}/\hbar = 0.0104$ Å^{-1} up to $r \sim 1200$ Å which is large enough for our discussions.

We recommend utilizing complex-range Gaussian basis functions e.g. when describing i) highly excited vibrational states, ii) discretization of continuum states [12], iii) amplitude of a scattering state in the interaction region [33], iv) strong short-range correlation and long-range asymptotic behavior.

2.4. Infinitesimally-shifted Gaussian lobe basis functions

In the calculations of the matrix elements of the Hamiltonian of three-body systems, particularly when complicated interactions are employed, integrations over all of the radial and angular coordinates become laborious even with Gaussian basis functions. The difficulty increases when we proceed to four-body problems. However, an important development [10,19,20] in our method was made by

Downloaded from https://academic.oup.com/ptep/article/2012/1/01A204/1565231 by University of Manchester user on 22 August 2022

introducing the infinitesimally-shifted Gaussian basis functions by

$$\phi_{nlm}(\mathbf{r}) = r^l e^{-\nu r^2} Y_{lm}(\hat{\mathbf{r}}) = \lim_{\varepsilon\to 0} \frac{1}{(\nu\varepsilon)^l} \sum_{k=1}^{k_{\max}} C_{lm,k}\, e^{-\nu(\mathbf{r}-\varepsilon \mathbf{D}_{lm,k})^2}. \tag{2.16}$$

The technique for determining the nondimensional parameters $\{C_{lm,k}, \mathbf{D}_{lm,k};\ k = 1 - k_{\max}\}$ is described in Appendix A.2 of Ref. [21]. Taking the limit $\varepsilon \to 0$ is to be carried out after the matrix elements have been calculated analytically. This new set of basis functions makes the calculation of three- and four-body matrix elements very easy. All the advantages of using the usual Gaussian basis functions remain with the new basis functions. With the use of these basis functions a variety of four-body calculations have been performed. Some of them will be reviewed in Sects. 3, 4, and 5.

Although the infinitesimally-shifted Gaussian basis functions are particularly useful in three- and four-body problems, it is instructive to show an example of calculating the matrix elements of a Gaussian potential $v_0\, e^{-\mu r^2}$ in the two-body case (see the Appendix of Ref. [21], concerning a technique for accurate and rapid computation of the three- and four-body matrix elements of two-body potentials with *arbitrary* shape). Integration over $\mathbf{r}$ is easily performed as

$$\langle \phi_{nlm}(\mathbf{r}) \mid v_0\, e^{-\mu r^2} \mid \phi_{n'lm}(\mathbf{r}) \rangle = v_0 \left(\frac{\pi}{\nu_n + \nu_{n'} + \mu}\right)^{3/2} \lim_{\varepsilon,\varepsilon'\to 0} \times \frac{1}{(\nu\nu'\varepsilon\varepsilon')^l} \sum_k \sum_{k'} C^*_{lm,k} C_{lm,k'} \exp\left[\frac{2\nu_n\nu_{n'}\varepsilon\varepsilon'}{\nu_n + \nu_{n'} + \mu} \mathbf{D}^*_{lm,k} \cdot \mathbf{D}_{lm,k'}\right], \tag{2.17}$$

where the term of ε^2 and that of ε'^2 in the $[\cdots]$ have already been removed since they vanish more rapidly, by $\varepsilon \to 0$ and $\varepsilon' \to 0$, than the term of $\varepsilon\varepsilon'$. If we take very small ε and ε' and compute Eq. (2.17) using the function subprogram for the $\exp[\cdots]$ part, we suffer from a serious round-off error in the summation over k and k' since terms of lower-order than $(\varepsilon\varepsilon')^l$ survive. If, instead, we expand the individual $\exp[\cdots]$ with respect to ε and ε', the terms with powers lower than $(\varepsilon\varepsilon')^l$ cancel out by the summation over k and k' due to the definition of our $C_{lm,k}$ and $C_{lm,k'}$. At the end of the calculation of Eq. (2.17) one is left only with a term proportional to $(\varepsilon\varepsilon')^l$ when $\varepsilon \to 0$ and $\varepsilon' \to 0$. Therefore, the $\exp[\cdots]$ part of Eq. (2.17) is replaced by

$$\frac{1}{l!}\left(\frac{2\nu_n\nu_{n'}\varepsilon\varepsilon'}{\nu_n + \nu_{n'} + \mu} \mathbf{D}^*_{lm,k} \cdot \mathbf{D}_{lm,k'}\right)^l. \tag{2.18}$$

Since the factor $(\varepsilon\varepsilon')^l$ in Eq. (2.18) cancels with the $(\varepsilon\varepsilon')^{-l}$ in Eq. (2.17), the two-body matrix element becomes independent of ε and ε' as

$$\langle \phi_{nlm}(\mathbf{r}) \mid v_0\, e^{-\mu r^2} \mid \phi_{nlm}(\mathbf{r}) \rangle = v_0 \frac{2^l \pi^{3/2}}{l!} \left(\frac{1}{\nu_n + \nu_{n'} + \mu}\right)^{l+3/2} \sum_k \sum_{k'} C^*_{lm,k} C_{lm,k'} (\mathbf{D}^*_{lm,k} \cdot \mathbf{D}_{lm,k'})^l. \tag{2.19}$$

This is, of course, too simple an example, but we remark the following advantage when applying this technique to three- or more-body systems: The RHS of Eq. (2.19) is a product of a term that depends only on the Gaussian size parameters and a term that is only a function of the shift coefficients. The latter can be calculated and stored prior to the matrix element calculation. Because this separation is also possible for three- and four-body matrix elements, the computation becomes very

Downloaded from https://academic.oup.com/ptep/article/2012/1/01A204/1565231 by University of Manchester user on 22 August 2022

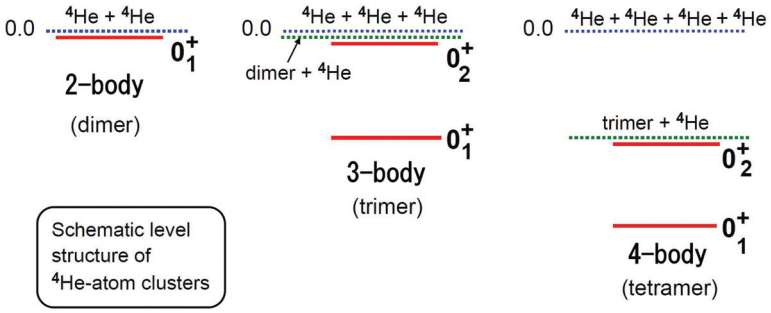

Fig. 7. Schematic level structure of ^{4}He-atom clusters (dimer, trimer, and tetramer), which is similar to the nuclear structure of α-clusters (^{8}Be, ^{12}C, and ^{16}O nuclei).

simple and efficient, as shown in Appendixes A.3 and A.4 of Ref. [21]. We do not need to perform complicated angular-momentum algebra (Racah algebra) due to the presence of many spherical harmonics functions. Use of the infinitesimally-shifted Gaussian lobe basis functions makes it possible for the present author and collaborators to have performed a variety of three- to five-body calculations reported and referred to in this paper.

We note that this method is available in the case of complex-range Gaussians and was actually used in the three- and four-body calculations in Refs. [34,35] (see the next section) as well as three-body reaction calculations in Ref. [33].

3. Universality in atomic and nuclear few-body systems: Application of GEM to three- and four-body ^{4}He-atom clusters

In this section, we apply GEM to three- and four-body ^{4}He-atom systems, referred to as the ^{4}He trimer and tetramer, respectively. The interaction between ^{4}He atoms has an extremely strong short-range repulsive core ($\sim 10^6$ K in height due to the Pauli principle between the closed-shell orbital electrons in each ^{4}He atom) followed by a weak attraction by the van der Waals potential (~ -10 K in depth). The interaction that has a scattering length (~ 100 Å) much larger than the interaction range (~ 5 Å) supports one shallow bound state (~ -1 mK). Therefore, ^{4}He clusters have similar properties to nuclear systems due to the universality [49–54] coming from the short-range interaction with large scattering length.

Since the ^{4}He–^{4}He interaction is a central potential with a strong repulsive core, the study of ^{4}He few-body systems provides good examples of computation for nuclear few-body systems as well as being of interest from the viewpoint of ultracold-atom physics [34–36,49–54].

According to recent studies of ^{4}He-atom clusters, especially precise three-body and four-body calculations by the present authors and collaborators [34–36], it becomes clear that the level structure of ^{4}He-atom clusters is similar to that of the nuclear α-cluster structure of ^{8}Be, ^{12}C, and ^{16}O nuclei (see Fig. 7) and is partially similar to the level structure of two-, three-, and four-nucleon systems (except that no three-nucleon excited state is evident).

A long-standing problem in the study of ^{4}He-atom cluters is the difficulty of obtaining a reliable four-body calculation of the excited state of the ^{4}He tetramer; this is because of the difficulty of describing the very weakly excited bound state below the trimer-atom threshold in the presence of the extremely strong short-range repulsive core; the four-body wave function should describe accurately the short-range structure ($r \lesssim 5$ Å) and the long-range asymptotic behavior (up to ~ 1000 Å).

Downloaded from https://academic.oup.com/ptep/article/2012/1/01A204/1565231 by University of Manchester user on 22 August 2022

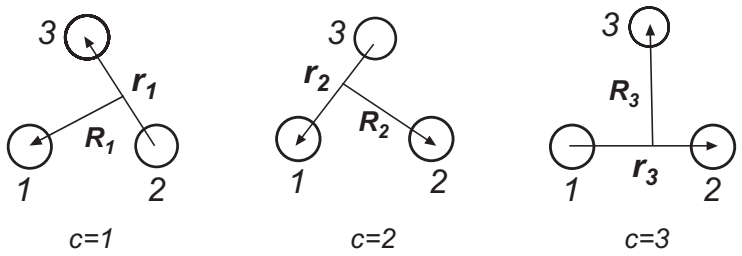

Fig. 8. Three sets of Jacobi coordinates of a three-body system.

This problem was solved by the application of GEM to the trimer and tetramer ground and excited states [34,35]. The GEM was found to be suitable for describing the strong short-range correlations and the long-range aymptotic behabior simultaneously. We shall explain, in this section, the important characteristics of ^{4}He-atom systems that were made clear by the accurate calculations. This will be instructive in the study of nuclear few-body systems.

3.1. Three-body Gaussian basis functions for identical spinless particles

We explain the GEM calculation for the three-body system interacting with central potentials, taking the case of the three-body system (trimer) of ^{4}He atoms, which are spinless identical bosons. We consider the three sets of Jacobi coordinates (Fig. 8). The Hamiltonian of the system is expressed as

$$H = -\frac{\hbar^2}{2\mu_{r_c}}\nabla^2_{r_c} - \frac{\hbar^2}{2\mu_{R_c}}\nabla^2_{R_c} + \sum_{1=i<j}^{3} V(r_{ij}), \tag{3.1}$$

where $c = 1$, 2, or 3 and $\mu_{r_c} = \frac{1}{2}m$ and $\mu_{R_c} = \frac{2}{3}m$, m being the mass of a ^{4}He atom. The conversion constant $\frac{\hbar^2}{m} = 12.12$ KÅ^2 is used. $V(r_{ij})$ is the two-body ^{4}He–^{4}He potential as a function of the pair distance $\mathbf{r}_{ij} = \mathbf{r}_j - \mathbf{r}_i$. In this section we employ the LM2M2 potential [47], which is one of the most widely used realistic ^{4}He–^{4}He potentials.

We calculate the three-body bound-state wave function, Ψ_3, which satisfies the Schrödinger equation

$$(H - E)\Psi_3 = 0. \tag{3.2}$$

We expand the wave function of three identical spinless bosons in terms of L^2-integrable, fully symmetric three-body basis functions:

$$\Psi_3 = \sum_{\alpha=1}^{\alpha_{\max}} C_\alpha \Phi_\alpha^{(\mathrm{sym})}, \tag{3.3}$$

$$\Phi_\alpha^{(\mathrm{sym})} = \Phi_\alpha(\mathbf{r}_1, \mathbf{R}_1) + \Phi_\alpha(\mathbf{r}_2, \mathbf{R}_2) + \Phi_\alpha(\mathbf{r}_3, \mathbf{R}_3). \tag{3.4}$$

It is of importance that these basis functions $\{\Phi_\alpha^{(\mathrm{sym})}; \alpha = 1, \ldots, \alpha_{\max}\}$, which are nonorthogonal to each other, are constructed on the full three sets of Jacobi coordinates; this makes the function space of $\{\Phi_\alpha^{(\mathrm{sym})}\}$ quite wide.

The eigenenergies E and amplitudes C_α of the ground and excited states are determined by the Rayleigh–Ritz variational principle:

$$\langle \Phi_\alpha^{(\mathrm{sym})} \mid H - E \mid \Psi_3 \rangle = 0, \qquad (\alpha = 1, \ldots, \alpha_{\max}), \tag{3.5}$$

Downloaded from https://academic.oup.com/ptep/article/2012/1/01A204/1565231 by University of Manchester user on 22 August 2022

which results in a generalized eigenvalue problem:

$$\sum_{\alpha'=1}^{\alpha_{\max}} \left[\mathcal{H}_{\alpha,\alpha'} - E\,\mathcal{N}_{\alpha,\alpha'}\right] C_{\alpha'} = 0. \qquad (\alpha = 1, \ldots, \alpha_{\max}). \tag{3.6}$$

The matrix elements are written as

$$\mathcal{H}_{\alpha,\alpha'} = \langle \Phi_{\alpha}^{(\mathrm{sym})} \mid H \mid \Phi_{\alpha'}^{(\mathrm{sym})} \rangle = 3\,\langle \Phi_{\alpha}(\mathbf{r}_1, \mathbf{R}_1) \mid H \mid \Phi_{\alpha'}^{(\mathrm{sym})} \rangle, \tag{3.7}$$

$$\mathcal{N}_{\alpha,\alpha'} = \langle \Phi_{\alpha}^{(\mathrm{sym})} \mid N \mid \Phi_{\alpha'}^{(\mathrm{sym})} \rangle = 3\,\langle \Phi_{\alpha}(\mathbf{r}_1, \mathbf{R}_1) \mid N \mid \Phi_{\alpha'}^{(\mathrm{sym})} \rangle. \tag{3.8}$$

The lowest-lying two S-wave eigenstates, $\Psi_3^{(v)}(v = 1, 2)$, will be identified as the trimer ground (0_1^+) and excited (0_2^+) states.

We express each basis function $\Phi_{\alpha}(\mathbf{r}_c, \mathbf{R}_c)$ as

$$\Phi_{\alpha}(\mathbf{r}_c, \mathbf{R}_c) = \phi_{nl}^{(\substack{\cos\\ \sin})}(r_c)\psi_{NL}(R_c)\Big[Y_l(\widehat{\mathbf{r}}_c)Y_L(\widehat{\mathbf{R}}_c)\Big]_{JM}, \tag{3.9}$$

where $\phi_{nl}^{(\substack{\cos\\ \sin})}(r)$ and $\psi_{NL}(R)$ are given by

$$\phi_{nl}^{(\substack{\cos\\ \sin})}(r) = r^l e^{-(r/r_n)^2} \times \begin{cases} \cos \omega (r/r_n)^2, \\ \sin \omega (r/r_n)^2, \end{cases} \qquad r_n = r_1\, a_r^{n-1}\ (n = 1, \ldots, n_{\max}) \tag{3.10}$$

$$\psi_{NL}(R) = R^L\, e^{-(R/R_N)^2}. \qquad R_N = R_1\, A_R^{N-1}\ (N = 1, \ldots, N_{\max}). \tag{3.11}$$

In Eq. (3.9), α specifies a set of quantum numbers,

$$\alpha = \{\cos \text{ or } \sin, \omega, nl, NL, JM\} \tag{3.12}$$

in common for the components $c = 1, 2, 3$. J is the total angular momentum and M is its z-component. In this work, we consider trimer bound states with $J = 0$ (there is no bound state with $J > 0$). Then, the totally symmetric three-body wave function requires $l = L =$ even.

The reason why complex-range Gaussian bases (3.10) are employed for the coordinate r is as follows: i) The repulsive core of the ^{4}He–^{4}He potential along r is extremely strong and therefore the short-range wave function exhibits a heavy suppression for $r \lesssim 2$ Å and a very steep increase for $2 \lesssim r \lesssim 4$ Å (see Figs. 6 and 9). Description of this behavior requires particularly appropriate basis functions. ii) The function space of the bases given by (3.10) is apparently wider than those given by (2.9) since the former have the oscillating degree of freedom. iii) The sine-type bases in particular work when the wave function is extremely suppressed at $r \sim 0$ due to the strongly repulsive short-range potential. iv) The wave function along R behaves so moderately that use of the real-range Gaussians is sufficient.

We further note that the short-range correlation due to the nucleon–nucleon potential is not as strong as that due to the present ^{4}He–^{4}He potential (compare the two-body correlation function of the four-nucleon ground state in Fig. 16 in Sect. 4 with that in Fig. 9 for the ^{4}He trimer and with that in Fig. 8 of Ref. [34] for the ^{4}He tetramer); it is, therefore, not necessary to use complex-range Gaussian basis functions for four-nucleon systems. We recommend first trying the case with real-range Gaussians for any few-body bound-state calculation and then trying complex-range Gaussians if the accuracy of the first result is not satisfactory for the purpose of the calculation. If the wave function has a radial oscillation with more than several nodes, use of complex-range Gaussian basis functions from the beginning is recommended.

Here, we make a remark about the generalized matrix eigenvalue problem (3.6). When the nonorthogonality of the large-size basis functions employed is not small enough, the solution of

Downloaded from https://academic.oup.com/ptep/article/2012/1/01A204/1565231 by University of Manchester user on 22 August 2022

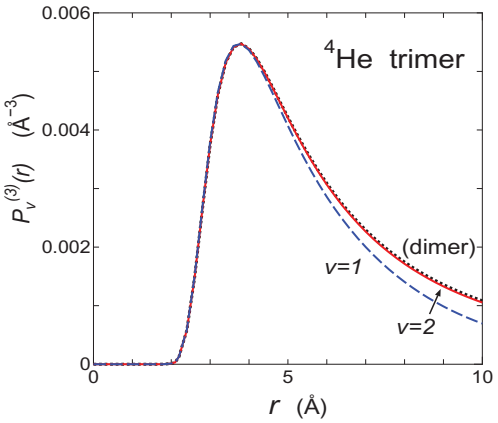

Fig. 9. Short-range structure of the pair correlation function $P_3^{(v)}(r)$ of the ^{4}He trimer calculated by (3.13). The dashed (blue) line is for the ground state ($v = 1$), the solid line (red) for the excited state ($v = 2$), and the dotted line for the ^{4}He dimer ($|\Psi_2(r)|^2$). The solid and dotted lines have been multiplied by factors 14.5 and 6.0, respectively, to be normalized at the peak.

Table 3. All the nonlinear parameters of the Gaussian basis functions used for the ^{4}He-trimer states with $J = 0\,(l = L)$. Those in column a) are commonly for $\phi_{nl}^{(\cos)}(r)$ and $\phi_{nl}^{(\sin)}(r)$ and b) for $\psi_{NL}(R)$. The total number of the basis, $\alpha_{\max}$, is 4400. This table is taken from Ref. [34].

a) $\phi_{nl}^{(\cos)}(r)$, $\phi_{nl}^{(\sin)}(r)$					b) $\psi_{NL}(R)$				
l	$n_{\max}$	r_1 (Å)	$r_{n_{\max}}$ (Å)	ω	L	$N_{\max}$	R_1 (Å)	$R_{N_{\max}}$ (Å)	Number of basis
0	22	0.3	150.0	1.0	0	50	0.4	600.0	2200
2	17	0.6	150.0	1.0	2	40	0.8	400.0	1360
4	14	0.8	130.0	1.0	4	30	1.0	200.0	840

Eq. (3.6) often becomes ill-conditioned due to round-off errors in the computation. For such cases we take a steady and accurate method that is often used in the literature. The method is precisely explained in Sects. II-H and III-B of Ref. [34].

3.2. *Results for the* ^{4}He *trimer*

The converged results of the three-body calculation were obtained by taking the symmetric three-body basis function $\{\Phi_\alpha^{(\mathrm{sym})}; \alpha = 1, \ldots, \alpha_{\max}\}$ with $\alpha_{\max} = 4400$, in which the shortest-range set is ($r_1 = 0.3$ Å, $R_1 = 0.4$ Å) and the longest-range one is ($r_{\max} = 150$ Å, $R_{\max} = 600$ Å). All the nonlinear parameters of the Gaussian basis set are listed in Table 3. The list is very small and there are neither additional parameters nor assumptions. The present three-body calculation is so transparent that it is possible for readers to repeat the calculation and check the results. The parameters for the Gaussian ranges are in round numbers but further optimization of them does not improve the binding energies ($B_3^{(1)} = 126.40$ mK and $B_3^{(2)} = 2.2706$ mK), as long as we calculate them with *five* significant figures.

Convergence of the binding energies $B_3^{(1)}$ and $B_3^{(2)}$ with respect to increasing partial waves $l\,(= L)$ is shown in Table 4 in comparison with the Faddeev-equation calculation by Lazauskas and Carbonell [55]. The case $l_{\max} = 4$ is sufficient in the present work as long as the accuracy of five significant digits is required. The convergence of the GEM result is more rapid than that of the Faddeev solution (the same is seen in the tetramer calculation [34]). The reason for this is that both

Downloaded from https://academic.oup.com/ptep/article/2012/1/01A204/1565231 by University of Manchester user on 22 August 2022

Table 4. Convergence of the ^{4}He trimer calculations with respect to the increasing maximum partial wave ($l_{\max}$). The four columns present trimer ground ($B_3^{(1)}$) and excited ($B_3^{(2)}$) state energies in comparison with those obtained by the Faddeev-equation calculation [55].

Trimer	GEM [34]		Faddeev equation [55]	
$l_{\max}$	$B_3^{(1)}$ (mK)	$B_3^{(2)}$ (mK)	$B_3^{(1)}$ (mK)	$B_3^{(2)}$ (mK)
0	121.00	2.2397	89.01	2.0093
2	126.39	2.2705	120.67	2.2298
4	126.40	2.2706	125.48	2.2622
8			126.34	2.2677
12			126.39	2.2680
14			126.39	2.2680

Table 5. Binding energies, $B_3^{(v)}(v = 1, 2)$, and mean values of the trimer ground and excited states by the GEM calculation [34] and the Faddeev-equation calculation [55] for the LM2M2 potential. r_{ij} stands for interparticle distance.

	Ground state (0_1^+)		Excited state (0_2^+)	
Trimer	GEM [34]	Ref. [55]	GEM [34]	Ref. [55]
$B_3^{(1)}$ (mK)	126.40	126.39	2.2706	2.268
$\langle T \rangle$ (mK)	1660.4	1658	122.15	122.1
$\langle V \rangle$ (mK)	−1786.8	−1785	−124.42	−124.5
$\sqrt{\langle r_{ij}^2 \rangle}$ (Å)	10.96	10.95	104.5	104.3
$\langle r_{ij} \rangle$ (Å)	9.616	9.612	84.51	83.53

the interaction and the wave function are truncated in the angular-momentum space ($l_{\max}$) in the Faddeev calculations, but the full interaction is included in the GEM calculation (with no partial-wave decomposition) though the wave function is truncated ($l_{\max}$). The difference of the convergence in the two calculation methods was precisely discussed in the case of three-nucleon bound states (^{3}H and ^{3}He nuclei) in our GEM calculation [8,9,21] and in a Faddeev-equation calculation [56].

Binding energies and some mean values of the trimer ground and excited states, calculated with GEM [34], are summarized in Table 5 in comparison with those obtained by the Faddeev equation method [55] (see Table 1 of Ref. [34] for other results reported in the literature). Our results agree excellently with those in the literature. The ^{4}He–^{4}He bond length in the trimer ground state was measured as $\langle r_{ij} \rangle = 11^{+4}_{-5}$ Å [48], which is well explained by our calculation, $\langle r_{ij} \rangle = 9.616$ Å. As illustrated in Fig. 7, the trimer excited state (0_2^+), which is known as an Efimov state [49–51], is located only 0.97 mK below the dimer-atom threshold (−1.303 49 mK).

In order to see how the present method describes the short-range structure of the trimer, we calculated the pair correlation function (pair distribution function or two-body density) $P_3^{(v)}(r)$ defined by

$$P_3^{(v)}(r)\, Y_{00}(\hat{\mathbf{r}}) = \langle\, \Psi_3^{(v)} \mid \delta(\mathbf{r} - \mathbf{r}_1) \mid \Psi_3^{(v)} \,\rangle_{\mathbf{r}_1, \mathbf{R}_1} \qquad (v = 1, 2). \tag{3.13}$$

$P_3^{(v)}(r)$ is apparently normalized as $\int P_3^{(v)}(r)\, r^2 \mathrm{d}r = 1$ and represents the probability of finding two particles at an interparticle distance r.

In Fig. 9, the short-range structure of $P_3^{(v)}(r)(v = 0, 1)$ is illustrated together with $P_2(r)(= |\Psi_2(r)|^2)$ for the ^{4}He dimer. The dashed (blue) line is for the trimer ground state ($v = 1$). The solid (red) line for the excited state ($v = 2$) and the dotted line for the dimer have been multiplied by factors 14.5 and 6.0, respectively. It is of interest that precisely the same shape of the short-range correlation ($r \lesssim 4$ Å) as seen in the dimer appears in both the trimer ground and excited states (the same is seen

Downloaded from https://academic.oup.com/ptep/article/2012/1/01A204/1565231 by University of Manchester user on 22 August 2022

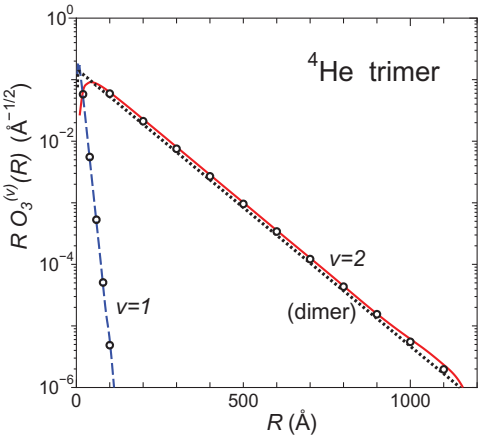

Fig. 10. Overlap function $\mathcal{O}_3^{(v)}(R)$, multiplied by R, between the ^{4}He trimer wave function ($v = 1, 2$) and the dimer one, which is defined by (3.14). Open circles represent the fit of the exact asymptotic function to $\mathcal{O}_3^{(v)}(R)$. The solid (red) line ($v = 2$) is found to be parallel to the dotted line for the dimer wave function ($R\Psi_2(R)$). This figure is taken from Ref. [34].

in the tetramer ground and excited states [34]). This gives a foundation to the a priori assumption that a two-particle correlation function (such as the Jastrow function) to simulate the short-range part of the dimer radial wave function $\Psi_2(r)$ is incorporated in the three-body wave function from the beginning.

To investigate the trimer configuration in the asymptotic region where one atom is far from the other two, we calculate the overlap function $\mathcal{O}_3^{(v)}(R_1)$ to describe the overlap between the trimer wave function $\Psi_3^{(v)}(v = 1, 2)$ and the dimer one $\Psi_2(\mathbf{r})$:

$$\mathcal{O}_3^{(v)}(R_1)\, Y_{00}(\hat{\mathbf{R}}_1) = \langle\, \Psi_2(\mathbf{r}_1) \mid \Psi_3^{(v)} \,\rangle_{\mathbf{r}_1} \qquad (v = 1, 2). \tag{3.14}$$

In Fig. 10, we plot $R\,\mathcal{O}_3^{(v)}(R)$ for the ground and excited states. They should asymptotically satisfy

$$y\,\mathcal{O}_3^{(v)}(R) \xrightarrow{R\to\infty} C_3^{(v)} \exp(-\kappa_3^{(v)} R),$$

where $\kappa_3^{(v)}$ is the binding wave number given by

$$\kappa_3^{(v)} = \sqrt{2\mu_R(B_3^{(v)} - B_2)}/\hbar \left(\kappa_3^{(1)} = 0.117\,\text{Å}^{-1}, \kappa_3^{(2)} = 0.0103\,\text{Å}^{-1}\right).$$

The asymptotic behavior with $C_3^{(1)} = 0.562\,\text{Å}^{-1/2}$ and $C_3^{(2)} = 0.179\,\text{Å}^{-1/2}$ (see the open circles) is precisely reproduced by the dashed (blue) line ($v = 1$) and the solid (red) line ($v = 2$), respectively, up to $\sim$1000 Å, which demonstrates the accuracy of our wave functions in the asymptotic region.

3.3. *Dimerlike-pair model for the* ^{4}He *trimer*

In this subsection, we show that the binding energy of the trimer excited state $B_3^{(2)}$ by the precise three-body calculation can be reproduced by a simple intuitive model, the dimerlike-pair model [34].

In Fig. 10, we find that the solid (red) line ($v = 2$) is parallel to the dotted line (dimer) up to $\sim$1000 Å; namely, $\kappa_3^{(2)}(= 0.0103\,\text{Å}^{-1})$ is almost the same as κ_2 (=0.0104 Å^{-1}). This agreement is not accidental, but can be understood using the dimerlike-pair model for the asymptotic behavior of the trimer excited state (Fig. 11a). The model indicates that i) particle a, located far from b and c, which are *loosely* bound (dimer), is little affected by the interaction between b and c, ii) therefore, the

Downloaded from https://academic.oup.com/ptep/article/2012/1/01A204/1565231 by University of Manchester user on 22 August 2022

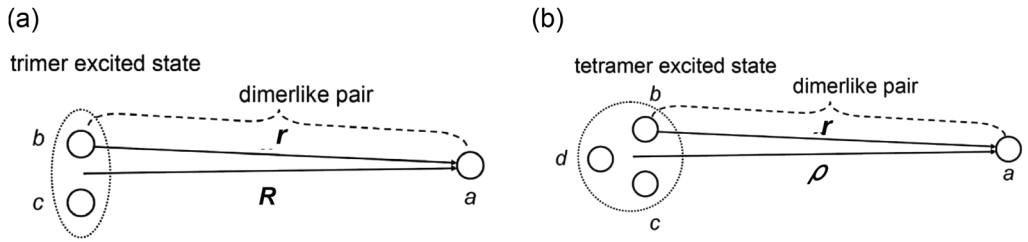

Fig. 11. Dimerlike-pair model for the asymptotic behavior of (a) the trimer excited state and (b) the tetramer excited states.

pair a and b at a distance r is asymptotically dimerlike, iii) since $\mathbf{r} \approx \mathbf{R}$ asymptotically, the amplitude of particle a along $\mathbf{R}$ is dimerlike, namely $\kappa_3^{(2)} \approx \kappa_2$.

Once we accept the dimerlike-pair model ($\kappa_3^{(2)} = \kappa_2$), we can estimate $\Delta B_3^{(2)} (= B_3^{(2)} - B_2)$, the binding energy of the trimer excited state with respect to the dimer, using B_2 only. Since we have $\kappa_2 = \sqrt{2\mu_r B_2}/\hbar$ and $\kappa_3^{(2)} = \sqrt{2\mu_R \Delta B_3^{(2)}}/\hbar$, where $\mu_r = \frac{1}{2}m$ and $\mu_R = \frac{2}{3}m$, we can predict

$$\Delta B_3^{(2)} = \frac{\mu_r}{\mu_R} B_2 = \frac{3}{4} B_2 = 0.978\,\text{mK}, \tag{3.15}$$

and hence the total binding energy $B_3^{(2)} = 2.281$ mK. These are close, respectively, to 0.967 mK and 2.2706 mK from the GEM three-body calculation.

Next, we apply the same model to the tetramer excited state [Fig. 11(b)] and predict its binding energy $\Delta B_4^{(2)} (= B_4^{(2)} - B_3^{(1)})$ with respect to the atom-trimer threshold ($B_3^{(1)}$). Asymptotically, particle a decays from the trimer $(b + c + d)$ as $\exp(-\kappa_4^{(2)}\rho)$ with $\kappa_4^{(2)} = \sqrt{2\mu_\rho \Delta B_4^{(2)}}/\hbar$, where $\mu_\rho = \frac{3}{4}m$ is the reduced atom-trimer mass. Taking $\kappa_4^{(2)} = \kappa_2$, we predict $\Delta B_4^{(2)}$ using B_2 only:

$$\Delta B_4^{(2)} = \frac{\mu_r}{\mu_\rho} B_2 = \frac{2}{3} B_2 = 0.87\,\text{mK} \tag{3.16}$$

and hence the total binding energy $B_4^{(1)} = 127.27$ mK. The values are close respectively to $\Delta B_4^{(2)} = 0.93$ mK and $B_4^{(2)} = 127.33$ mK, which will be shown in Sect. 3.4 by the four-body calculation. This demonstrates the validity of the dimerlike-pair model in the prediction of the tetramer excited-state energy. We note that, in the above estimation of the numerical values, we used the LM2M2 potential. In Sect. 3.6, using various realistic ^{4}He potentials, we shall discuss the correlation between the trimer and tetramer energies as well as the validity of the dimerlike-pair model.

3.4. Four-body Gaussian basis functions for identical spinless four particles

We take two types of Jacobi coordinate sets, K-type and H-type (Fig. 12). The total symmetrization between four bosonic particles generates the Jacobi coordinate sets $c = 1, \ldots, 12$ for the K-type and $c = 13, \ldots, 18$ for the H-type. An explicit illustration of the full 18 sets for four-body systems is seen in Fig. 18 of Ref. [21].

The four-body wave function Ψ_4 is obtained by solving the Schrödinger equation

$$(H - E)\Psi_4 = 0 \tag{3.17}$$

with the Hamiltonian

$$H = -\frac{\hbar^2}{2\mu_r}\nabla_r^2 - \frac{\hbar^2}{2\mu_R}\nabla_R^2 - \frac{\hbar^2}{2\mu_\rho}\nabla_\rho^2 + \sum_{1=i<j}^{4} V(r_{ij}), \tag{3.18}$$

Downloaded from https://academic.oup.com/ptep/article/2012/1/01A204/1565231 by University of Manchester user on 22 August 2022

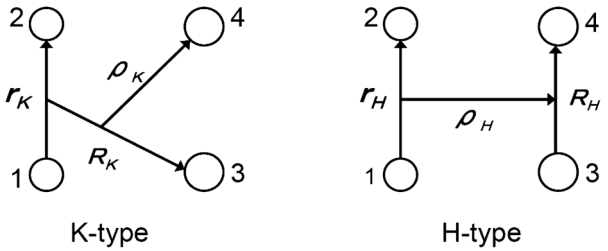

Fig. 12. K-type and H-type Jacobi coordinates for symmetric four-body systems. Symmetrization of the four particles generates the sets $c = 1, \ldots, 12$ (K-type) and $c = 13, \ldots, 18$ (H-type). See Fig. 18 of Ref. [21] for explicit figures for the 18 sets.

where $\mu_r = \frac{1}{2}m$, $\mu_R = \frac{2}{3}m$, and $\mu_\rho = \frac{3}{4}m$ on the K-type coordinates, and $\mu_r = \mu_R = \frac{1}{2}m$ and $\mu_\rho = m$ on the H-type ones.

The wave function Ψ_4 is expanded in terms of the symmetrized L^2-integrable K-type and H-type four-body basis functions:

$$\Psi_4 = \sum_{\alpha_K=1}^{\alpha_K^{\max}} A_{\alpha_K}^{(K)} \mathcal{S}\Phi_{\alpha_K}^{(K)}(\mathbf{r}_K, \mathbf{R}_K, \boldsymbol{\rho}_K) + \sum_{\alpha_H=1}^{\alpha_H^{\max}} A_{\alpha_H}^{(H)} \mathcal{S}\Phi_{\alpha_H}^{(H)}(\mathbf{r}_H, \mathbf{R}_H, \boldsymbol{\rho}_H), \tag{3.19}$$

where the symmtric basis functions $\mathcal{S}\Phi_{\alpha_K}^{(K)}$ and $\mathcal{S}\Phi_{\alpha_H}^{(H)}$ are given by

$$\mathcal{S}\Phi_{\alpha_K}^{(K)}(\mathbf{r}_K, \mathbf{R}_K, \boldsymbol{\rho}_K) = \sum_{c=1}^{12} \Phi_{\alpha_K}^{(K)}(\mathbf{r}_c, \mathbf{R}_c, \boldsymbol{\rho}_c), \tag{3.20}$$

$$\mathcal{S}\Phi_{\alpha_H}^{(H)}(\mathbf{r}_H, \mathbf{R}_H, \boldsymbol{\rho}_H) = \sum_{c=13}^{18} \Phi_{\alpha_H}^{(H)}(\mathbf{r}_c, \mathbf{R}_c, \boldsymbol{\rho}_c). \tag{3.21}$$

The eigenenergies E and amplitudes $A_{\alpha_K}^{(K)}(A_{\alpha_H}^{(H)})$ are determined by the Rayleigh–Ritz variational principle in the same manner as Eqs. (3.5)–(3.8).

We describe the basis function $\Phi_{\alpha_\mathrm{K}}^{(\mathrm{K})}(\Phi_{\alpha_\mathrm{H}}^{(\mathrm{H})})$ in the form

$$\Phi_{\alpha_\mathrm{K}}^{(\mathrm{K})}(\mathbf{r}_c, \mathbf{R}_c, \boldsymbol{\rho}_c) = \phi_{nl}^{(\cos_{\sin})}(r_c)\, \phi_{NL}(R_c)\, \varphi_{\nu\lambda}(\rho_c) \Big[\big[Y_l(\widehat{\mathbf{r}}_c) Y_L(\widehat{\mathbf{R}}_c) \big]_\Lambda Y_\lambda(\widehat{\boldsymbol{\rho}}_c) \Big]_{JM}, \tag{3.22}$$

$$\Phi_{\alpha_\mathrm{H}}^{(\mathrm{H})}(\mathbf{r}_c, \mathbf{R}_c, \boldsymbol{\rho}_c) = \phi_{nl}^{(\cos_{\sin})}(r_c)\, \phi_{NL}(R_c)\, \varphi_{\nu\lambda}(\rho_c) \Big[\big[Y_l(\widehat{\mathbf{r}}_c) Y_L(\widehat{\mathbf{R}}_c) \big]_\Lambda Y_\lambda(\widehat{\boldsymbol{\rho}}_c) \Big]_{JM}, \tag{3.23}$$

where α_K specifies a set

$$\alpha_\mathrm{K} \equiv \{\text{'cos' or 'sin'}, \omega, nl, NL, \nu\lambda, \Lambda, JM\}, \tag{3.24}$$

which is the same for the components $c = 1, \ldots, 12$; and similarly for α_H commonly for all $c = 13, \ldots, 18$.

Since we consider the case of $J = 0$ in this paper, the totally symmetric four-body wave function requires i) l = even, $L + \lambda$ = even, and $\Lambda = \lambda$ for the K-type basis and ii) l = even, L = even, and $\Lambda = \lambda$ = even for the H-type basis.

In (3.22) and (3.23), the radial functions are assumed, as in Sect. 3.1, to be

$$\phi_{nl}^{(\cos_{\sin})}(r) = r^l e^{-(r/r_n)^2} \times \begin{cases} \cos \omega (r/r_n)^2 \\ \sin \omega (r/r_n)^2 \end{cases}, \qquad r_n = r_1\, a_r^{n-1} (n = 1, \ldots, n_{\max}) \tag{3.25}$$

$$\psi_{NL}(R) = R^L e^{-(R/R_N)^2}, \qquad R_N = R_1\, A_R^{N-1} (N = 1, \ldots, N_{\max}) \tag{3.26}$$

$$\varphi_{\nu\lambda}(\rho) = \rho^\lambda e^{-(\rho/\rho_\nu)^2}, \qquad \rho_\nu = \rho_1\, \alpha_\rho^{\nu-1} (\nu = 1, \ldots, \nu_{\max}). \tag{3.27}$$

Downloaded from https://academic.oup.com/ptep/article/2012/1/01A204/1565231 by University of Manchester user on 22 August 2022

Table 6. Binding energies, $B_4^{(v)}(v = 1, 2)$, and mean values of the tetramer ground and excited states by the GEM calculation [34] and the Faddeev–Yakubovsky equation calculation [55] with the use of the LM2M2 potential. r_{ij} stands for interparticle. The numbers in parentheses were derived from the scattering calculation [55].

	Ground state (0_1^+)		Excited state (0_2^+)	
Tetramer	GEM [34]	Ref. [55]	GEM [34]	Ref. [55]
$B_4^{(1)}$ (mK)	558.98	557.73	127.33	(127.5)
$\langle T \rangle$ (mK)	4282.2	4107	1639.2	
$\langle V \rangle$ (mK)	−4841.2	−4665	−1766.5	
$\sqrt{\langle r_{ij}^2 \rangle}$ (Å)	8.43	8.40	54.5	(34.4)
$\langle r_{ij} \rangle$ (Å)	7.70		35.8	

In the tetramer calculation, the total number, $\alpha_{\max} = \alpha_{\mathrm{K}}^{\max} + \alpha_{\mathrm{H}}^{\max}$, of the symmetrized four-body basis functions (3.22) and (3.23) amount to $\alpha_{\max} = 29056$, ranging from very compact to very diffuse, to obtain a well converged solution (see Ref. [34] for convergence of the binding energies with respect to the increasing maximum partial waves (Table 4) and for the nonlinear parameters of the basis functions (Table 3)).

Calculated binding energies and some mean values of the tetramer ground and excited states are summarized in Table 6 in comparison with those obtained by the Faddeev–Yakubovsky equation method [55]. In the latter calculation [55], the excited state was not obtained by a direct bound-state calculation but was extrapolated from the atom-trimer scattering calculations. Our result of $B_4^{(1)} = 127.33\,\mathrm{mK}$ [34], which is very closed to $B_4^{(1)}$ obtained in Ref. [55], confirmed the existence of the very shallow $J = 0_2^+$ bound excited state of the ^{4}He tetramer (only 0.93 mK below the trimer-atom threshold at −126.40 mK, as illustrated in Fig. 7).

This excited state is considered to have a well developed clustering configuration composed of the trimer-like core and a distant fourth atom. To see the degree of clusterization, we calculate the overlap function (reduced width amplitude) between a tetramer state $\Psi_4^{(v)}(v = 1, 2)$ and the trimer ground state $\Psi_3^{(1)}$, similarly to Eq. (3.14):

$$\mathcal{O}_4^{(v)}(\rho_1)\, Y_{00}(\widehat{\boldsymbol{\rho}}_1) = \langle\, \Psi_3^{(1)} \mid \Psi_4^{(v)} \,\rangle_{\mathbf{r}_1, \mathbf{R}_1}. \tag{3.28}$$

In Fig. 13, the fourth atom is located close to the other three atoms in the ground state, but it is far away from them in the excited state. We confirm that the excited state has a very dilute trimer-atom clustering structure. We shall present in Sect. 4.2 the idea that, in the four-nucleon system, the excited state (0_2^+) is such a very dilute state composed of a three-nucleon cluster and a distant nucleon (see Fig. 17); this might be a universal property of the system interacting with large scattering length.

The strong short-range correlations ($r \lesssim 4$ Å) and long-range asymptotic behavior (up to ∼1000 Å) of the wave functions of the tetramer states, which are similar to those of the trimer states mentioned in Sect. 3.2, are seen in Figs. 8 to 11 in Ref. [34].

3.5. Universality in three- and four-body systems

Correlations between the binding energies in three- and four-body systems were first observed in nuclear physics and are known as the Tjon line [57], which refers to the approximately linear correlation between the binding energies of the triton and the alpha particle (namely, in our notation, the correlation between $B_3^{(1)}$ and $B_4^{(1)}$ when various nucleon–nucleon (NN) potentials are employed).

Downloaded from https://academic.oup.com/ptep/article/2012/1/01A204/1565231 by University of Manchester user on 22 August 2022

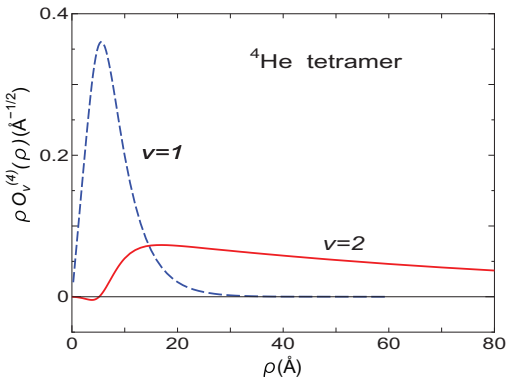

Fig. 13. Overlap function $\mathcal{O}_4^{(v)}(\rho)$ in (3.28) between (2.14) the trimer ground state and the tetramer state ($v = 1, 2$) as a function of the atom–trimer distance ρ. Note that similar behavior is seen in four-nucleon states (Fig. 14). Taken from Ref. [34].

Recently, the nuclear Tjon line was discussed in the context of the effective field theory of short-range interactions and low-momentum NN potentials [58,59]. The Tjon lines for the ^{4}He trimer and tetramers were investigated in Refs. [53,54] over the range of binding energies relevant to ^{4}He atoms on the basis of leading-order effective theory. But, due to scarce calculations of the tetramer excited-state binding energy $B_4^{(2)}$ at that time, the correlations associated with $B_4^{(2)}$ remained unexplored. However, we solved this problem in Ref. [34].

We considered all six kinds of correlations between two of the four binding energies, $B_3^{(1)}$, $B_3^{(2)}$, $B_4^{(1)}$, and $B_4^{(2)}$ that are calculated using the fourteen ^{4}He potentials (see Ref. [34] for a list of the potentials). Figures 14a to 14d illustrate the four kinds of correlations between the ground- and excited-state binding energies of the ^{4}He trimer and tetramer. The 14 data points are given by the GEM calculation for 14 various potentials. The dotted (red) lines in Fig. 14 are obtained by linear least squares fitting to the data points (the fitted linear functions are given in Ref. [34], including the $B_3^{(1)}$–$B_3^{(2)}$ and $B_4^{(1)}$–$B_4^{(2)}$ correlations). All the correlations are perfectly linear; this universal property for the various ^{4}He potentials has been discovered for the first time. It was really unexpected that all the calculated results (the data points) fell so beautifully on a straight line; we emphasize that the results are obtained by using *different* potentials, not by changing a parameter in a specific potential.

The solid lines in Fig. 14 illustrate the universal scaling functions relating the ^{4}He tetramer energies to the trimer energies, which were calculated by leading-order effective theory for the ^{4}He atoms (see Ref. [54] for details).

It is of interest to note that the slope of the Tjon line, the dotted (red) line in Fig. 14d, for the correlation between trimer and tetramer ground-state binding energies is 4.778 (see Eq. (4.4) in Ref. [35]), which is close to the slope of the nuclear Tjon line, ≈ 5.0 (see Fig. 2 in Ref. [58]).

3.6. *Dimerlike-pair model for the* ^{4}He *tetramer*

The dimerlike-pair model predicted, in Sect. 3.3, the relation $\Delta B_4^{(2)} = \frac{2}{3} B_2$ (Eq. (3.16)), which can be rewritten as

$$\frac{B_4^{(2)}}{B_2} = \frac{B_3^{(1)}}{B_2} + \frac{2}{3}. \tag{3.29}$$

This is shown in Fig. 14b with the dashed (blue) line, which is close to the 14 data points with almost the same quality of the dotted (red) line of the least squares fit. This relation is must be the simplest (but accurate) universal property of weakly bound cluster systems.

Downloaded from https://academic.oup.com/ptep/article/2012/1/01A204/1565231 by University of Manchester user on 22 August 2022

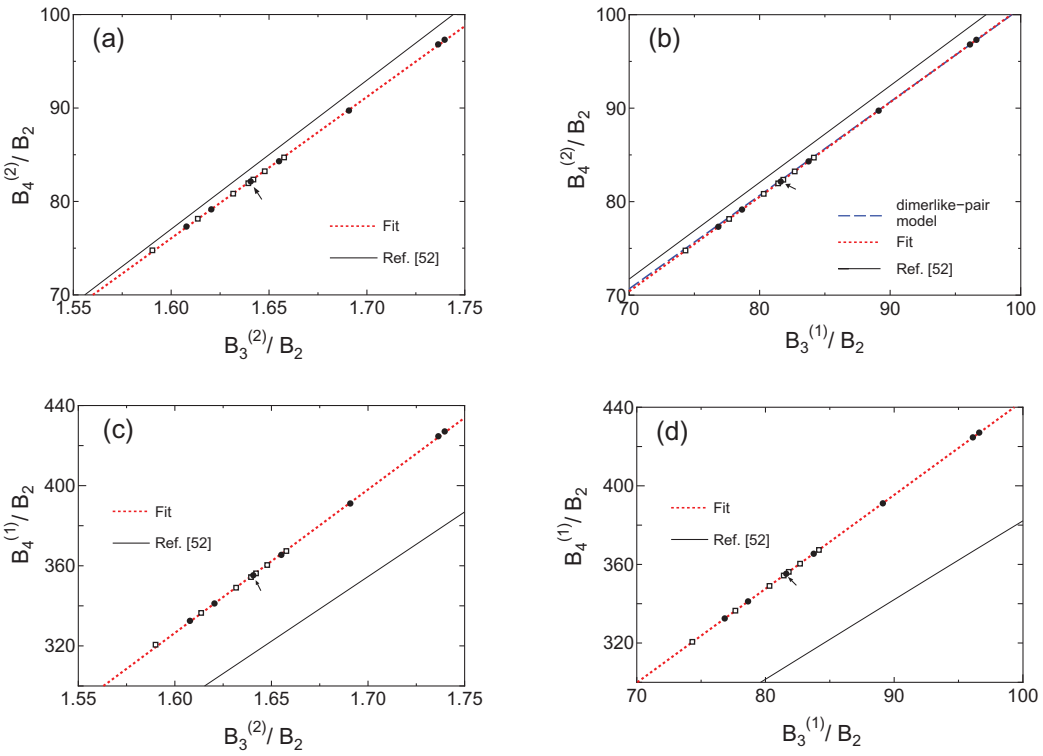

Fig. 14. The correlations between the ground- and excited-state binding energies of the ^{4}He trimer and tetramer. a) and c): $B_4^{(2)}$ and $B_4^{(1)}$ as a function of $B_3^{(2)}$. b) and d): the same quantities as a function of $B_3^{(1)}$. The energies are normalized by the dimer energy B_2. All 14 data points are obtained by the three- and four-body calculation using various ^{4}He potentials (see Ref. [35] for details). The dotted (red) linear line is the linear least squares fit to the 14 data points. The dashed (blue) line in b) is the prediction from the dimerlike-pair model, Eq. (3.29). The solid line, taken from Ref. [54], shows the universal scaling curve obtained from leading-order effective theory. This figure is taken from Ref. [35].

Generally, in the case of $^4\mathrm{He}_N$, N-atom clusters, the model suggests that the excited-state binding energy may be presented as $\frac{B_N^{(2)}}{B_2} = \frac{B_{N-1}^{(1)}}{B_2} + \frac{N}{2(N-1)}$, where the last term is the ratio of the reduced mass of the dimerlike pair ($\frac{1}{2}m$) to that of the ^{4}He–$^4\mathrm{He}_{N-1}$ system ($\frac{N-1}{N}m$).

4. Application to four-nucleon systems: Completeness of four-body Gaussian basis functions

Calculation of the four-nucleon bound state (^{4}He) using realistic NN force is useful for testing the method and the scheme of the calculation. In 2001, a benchmark test calculation of the four-body bound state was performed in Ref. [29] by eighteen authors, including the present author, from seven research groups with the use of the efficient calculation methods, namely, the Faddeev–Yakubovsky equation method (FY), the Gaussian expansion method (GEM), the stochastic variational method (SVM), the hyperspherical harmonic variational method (HH), the Green's function Monte Carlo (GFMC) method, the no-core shell model (NCSM), and the effective interaction hyperspherical harmonic method (EIHH) (see Ref. [29] for an extensive list of references for these methods). They used the NN realistic force, AV8′ interaction [60], and compared the calculated energy eigenvalues and some wave function properties.

The ^{4}He nucleus is the lightest nucleus that exhibits excited states (resonances). The first excited state (0_2^+) at $E_\mathrm{x} = 20.21$ MeV has the same spin, isospin, and parity as the ground state. Therefore,

Downloaded from https://academic.oup.com/ptep/article/2012/1/01A204/1565231 by University of Manchester user on 22 August 2022

the 0_2^+ state should have quite a different spatial structure in order to be orthogonal to the 0_1^+ state. The second 0^+ state in ^{4}He is then the smallest system in which one can study nuclear spatial excitation using realistic interactions. The question of the structural properties of the ^{4}He 0_2^+ state has since been the subject of numerous theoretical studies. Along this line, one of the next challenging projects is to calculate the properties of the second 0^+ state of ^{4}He using realistic interactions. One must reproduce simultaneously the ground state and the excited state, which have the same spin, isospin, and parity but possess quite different spatial structure; in this context, it is of importance to reproduce the observed form factor of the inelastic electron scattering $^4\mathrm{He}(e, e')^4\mathrm{He}(0_2^+)$. This problem was solved in Ref. [30] by the present author and collaborators.

In this section, i) we briefly review, in Sect. 4.1, the result of the above benchmark test calculation [29] and ii) we present, in Sect. 4.2, the GEM four-body calculation [30] of the first excited state ($T = 0, 0_2^+$) at $E_\mathrm{x} = 20.21$ MeV and discuss the completeness of the four-body Gaussian basis functions.

4.1. Four-nucleon ground state $^4\mathrm{He}(0_1^+)$

In GEM, the total four-body wave function is given as a sum of the component functions of all the Jacobi-coordinate rearrangement channels within the LS coupling scheme with the K-type and H-type configurations (Fig. 15):

$$\Psi_{J=0} = \sum_\alpha C_\alpha^{(K)} \Phi_\alpha^{(K)} + \sum_\alpha C_\alpha^{(H)} \Phi_\alpha^{(H)}, \tag{4.1}$$

where the anti-symmetrized basis functions are described by

$$\begin{aligned}\Phi_\alpha^{(K)} = \mathcal{A}\Big\{\Big[\Big[[\phi_{nl}(\mathbf{r}_K)\psi_{NL}(\mathbf{R}_K)]_\Lambda\, \varphi_{\nu\lambda}(\boldsymbol{\rho}_K)\Big]_I\, \big[[\chi_s(12)\chi_{\frac{1}{2}}(3)]_{s'}\chi_{\frac{1}{2}}(4)\big]_S\Big]_{JM} \\ \times \big[[\eta_t(12)\eta_{\frac{1}{2}}(3)]_{\frac{1}{2}}\eta_{\frac{1}{2}}(4)\big]_0\Big\},\end{aligned} \tag{4.2}$$

$$\begin{aligned}\Phi_\alpha^{(H)} = \mathcal{A}\Big\{\Big[\Big[[\phi_{nl}(\mathbf{r}_H)\psi_{NL}(\mathbf{R}_H)]_\Lambda\, \varphi_{\nu\lambda}(\boldsymbol{\rho}_H)\Big]_I\, \big[\chi_s(12)\chi_{s'}(34)\big]_S\Big]_{JM} \\ \times \big[\eta_t(12)\eta_t(34)\big]_0\Big\},\end{aligned} \tag{4.3}$$

with $\alpha \equiv \{nl, NL, \Lambda, \nu\lambda, I, ss'S, t\}$. Radial parts of the spatial functions are taken to be real-range Gaussian basis functions with the ranges in geometric progressions:

$$\phi_{nl}(r) = r^l e^{-(r/r_n)^2}, \qquad r_n = r_1\, a_r^{n-1} (n = 1, \ldots, n_\mathrm{max}) \tag{4.4}$$

$$\psi_{NL}(R) = R^L e^{-(R/R_N)^2}, \qquad R_N = R_1\, A_R^{N-1}\ (N = 1, \ldots, N_\mathrm{max}) \tag{4.5}$$

$$\varphi_{\nu\lambda}(\rho) = \rho^\lambda e^{-(\rho/\rho_\nu)^2}, \qquad \rho_\nu = \rho_1\, \alpha_\rho^{\nu-1}\ (\nu = 1, \ldots, \nu_\mathrm{max}). \tag{4.6}$$

Due to the four-nucleon antisymmetrizer $\mathcal{A}$, K-type includes the Jacobi coordinate sets $c = 1$ to 12 and H-type the sets $c = 13$ to 18 (See Fig. 18 in Ref. [21] for the full 18 sets of the Jacobi coordinates of four-body systems). χ and η are the spin and isospin functions, respectively. Eigenenergies and wave function coefficients, C_α, are determined by the Rayleigh–Ritz variational principle. The angular momentum space of $l, L, \lambda \leq 2$ is found to be enough to get sufficient convergence of the calculated results mentioned below.

In Table 7, calculated values of the binding energy E and the r.m.s. radius are compared between the seven methods. Good agreement for E is within 3 digits or within 0.5%. This is quite remarkable in view of the very different techniques of calculation and the complexity of the nuclear force chosen.

Downloaded from https://academic.oup.com/ptep/article/2012/1/01A204/1565231 by University of Manchester user on 22 August 2022

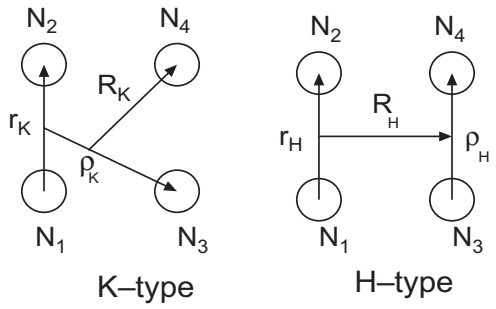

Fig. 15. K-type and H-type Jacobi coordinates for the four-nucleon systems. Antisymmetrization of the four particles generates the Jacobi coordinate sets $c = 1, \ldots, 12$ (K-type) and $c = 13, \ldots, 18$ (H-type). See Fig. 18 of Ref. [21] for explicit figures for the 18 sets.

Table 7. Calculated results for ^{4}He properties by seven methods of calculation. Taken from Ref. [29] (note that the GEM was referred to as CRC-GV in Ref. [29]).

Method	E (MeV)	$\sqrt{\langle r^2 \rangle}$ (fm)	S (%)	P (%)	D (%)
FY	−25.94(5)	1.485(3)	85.71	0.38	13.91
GEM	−25.90	1.482	85.73	0.37	13.90
SVM	−25.92	1.486	85.72	0.368	13.91
HH	−25.90(1)	1.483	85.72	0.369	13.91
GFMC	−25.93(2)	1.490(5)			
NCSM	−25.80(20)	1.485	86.73	0.29	12.98
EIHH	−25.944(10)	1.486	85.73	0.370(1)	13.89

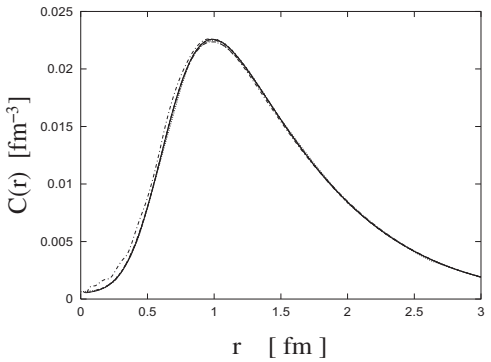

Fig. 16. Correlation functions of ^{4}He in the different calculational schemes: FY, GEM, SVM, HH, and NCSM (overlapping curves) and EIHH (dash-dotted curve), except GFMC. Taken from Ref. [29].

The radius is also in good agreement between the seven methods. Table 7 also shows the probabilities of finding three different total orbital angular momentum components. Agreement between the different groups is good.

As a more detailed test of the calculated wave functions, we show the NN correlation function (two-body density)

$$C(r) = \langle \Psi_{J=0} | \delta(\mathbf{r} - \mathbf{r}_{ij}) | \Psi_{J=0} \rangle, \tag{4.7}$$

where $\mathbf{r}_{ij}$ is the distance between particles i and j. It is normalized as $4\pi \int C(r) r^2 d\mathrm{r} = 1$. The results obtained by the various calculational schemes are shown in Fig. 16. The agreement between the FY, GEM, SVM, HH, and NCSM is essentially perfect.

Downloaded from https://academic.oup.com/ptep/article/2012/1/01A204/1565231 by University of Manchester user on 22 August 2022

In conclusion, the results of all schemes agree very well, showing the high accuracy of the existing methods of calculation of the four-nucleon bound state.

4.2. Structure of the four-nucleon second 0^+ *state* $^4\mathrm{He}(0_2^+)$

In investigating the spatial structure of the ^{4}He 0_2^+ state, it is particularly important to explain the observed (e, e') transition form factor. Moreover, from analyzing the low-momentum-transfer part of the form factor, it was reported that only about 11% of the energy-weighted (EW) $E0$ sum rule limit was exhausted by the second 0^+ state [61,62]. In medium-heavy or heavy nuclei, normally 80–90% of the limit is exhausted by the second 0^+ state because it is a collective, breathing mode. For the ^{4}He nucleus, one should understand where the major component of the sum rule value is situated.

Precisely speaking, the second 0^+ state is a resonance lying above the $^3\mathrm{H} + p$ threshold ($E_\mathrm{x} = 19.815$ MeV). But it lies below both the top of the $^3\mathrm{H} + p$ Coulomb barrier ($\sim$0.88 MeV) and the $^3\mathrm{He} + n$ threshold ($E_\mathrm{x} = 20.578$ MeV), located at the mean position of the two thresholds. The width of this s-wave resonance is rather small (500 keV). Therefore, if an isospin formalism is employed for ^{4}He, the $T = 0, 0_2^+$ state can be treated as a bound state; indeed, we took the formalism in Ref. [30] and obtained the $T = 0, 0_2^+$ state as a bound state below the calculated $T = 0$ (averaged) threshold. Therefore, this approximate treatment of the asymptotic behaviour of the 0_2^+ state is reasonable as long as one is discussing the transition $^4\mathrm{He}(e, e')^4\mathrm{He}(0_2^+)$ from the ground state, which has a short-range tail.

In order to investigate the (e, e') form factor and the spatial structure difference between the 0_1^+ and 0_2^+ states, it is necessary to reproduce with sufficient accuracy their energies (-28.30 MeV and -8.09 MeV) as well as the energies of ^{3}H and ^{3}He. For the NN interaction, we employed the AV8′ force [60], which is the same as that used in the benchmark test calculation of the ground state [29]. Because the use of two-body forces alone (the AV8′ potential plus Coulomb force) does not reproduce the binding energies of the ^{3}H, ^{3}He, and ^{4}He (0_1^+), we introduce a phenomenological *NNN* force with a two-range Gaussian form (see Ref. [30] for details). A sophisticated, spin-dependent *NNN* force is not necessary for the present purpose (to discuss the spatial structure of the 0_1^+ and 0_2^+ states); to reproduce the binding energy is essential, so that the wave functions have the correct asymptotic behavior. It is possible to adjust the *NNN* force parameters so as to reproduce simultaneously the binding energies of ^{3}H, ^{3}He, and $^4\mathrm{He}(0_1^+)$ within the desired accuracy [30].

There are no additional adjustable parameters in the calculation. The issues we address are then: i) whether the energy of the second 0^+ state is reproduced, ii) whether the (e, e') form factor is reproduced, and iii) where the major contribution to the EW $E0$ sum rule is.

The calculated energy of the second 0^+ state agrees well with the observed value. In the present isospin formalism, the 0_2^+ state is very weakly bound with respect to the theoretical $3N + N$ threshold, $E(3N) = -8.08$ MeV.

An effective way to investigate the spatial structure of the 0_1^+ and 0_2^+ states is to calculate the overlap amplitude between the $^4\mathrm{He}(0^+)$ and ^{3}H wave function:

$$\mathcal{Y}_{0_n^+}(R_\mathrm{K}) = \left\langle \left[\Phi_{\frac{1}{2}}^{(^3\mathrm{H})}(1,2,3) Y_0(\widehat{R}_\mathrm{K}) \chi_{\frac{1}{2}}(4) \right]_{0^+} \eta_{\frac{1}{2},-\frac{1}{2}}(4) | \Psi_{0_n^+}(1,2,3,4) \right\rangle, \tag{4.8}$$

where $\boldsymbol{\rho}_\mathrm{K}$ is the position vector of particle 4 with respect to the c.m. of particles 1–3 (see K-type in Fig. 15). $\Phi_{\frac{1}{2}}^{(^3\mathrm{H})}(123)$ is the ^{3}H wave function and $\chi_{\frac{1}{2}}(4)$ and $\eta_{\frac{1}{2}}(4)$ are the spin and isospin wave functions of particle 4, respectively. The overlap amplitudes $\mathcal{Y}_{0_n^+}(R_\mathrm{K})$ for the 0_1^+ and 0_2^+ states are illustrated in Fig. 17. In the ground state, the fourth nucleon is located close to the other three nucleons,

Downloaded from https://academic.oup.com/ptep/article/2012/1/01A204/1565231 by University of Manchester user on 22 August 2022

Table 8. Energies and wave function properties of the 0_1^+ and 0_2^+ states of ^{4}He calculated using GEM with the AV8′ NN force, the Coulomb force, and a phenomenological three-body force [30]. The numbers in parentheses are experimental values. In the isospin formalism, $E(3N)$ is the average energy of ^{3}H and ^{3}He, −8.08 (−8.10) MeV. This table is taken from Ref. [30].

^{4}He	0_1^+	0_2^+
E (MeV)	−28.44 (−28.30)	−8.19 (−8.09)
$E - E(3N)$ (MeV)	−20.36 (−20.20)	−0.11 (+0.01)
E_x (MeV)	0.0 (0.0)	20.25 (20.21)
P_S (%)	85.54	91.18
P_P (%)	0.38	0.08
P_D (%)	14.08	8.74
$\langle r_p^2 \rangle^{\frac{1}{2}}$ (fm)	1.660 (1.671 ± 0.014)	5.3
$\langle 0_2^+ \vert \Sigma_p r_p^2 \vert 0_1^+ \rangle$ (fm^2)		1.38 (1.10 ± 0.16 [61,62])

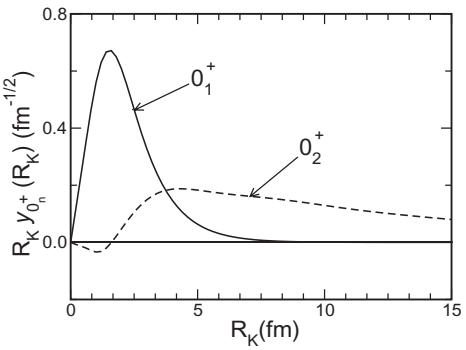

Fig. 17. The overlap amplitude between the ^{4}He (0_n^+) wave function and the ^{3}H wave function as defined by Eq. (4.8). Note that similar behavior is seen in the ^{4}He-atom tetramer (Fig. 13). Taken from Ref. [30].

but it is far away from them in the second 0^+ state. This loosely coupled $3N + N$ clustering property of the 0_2^+ state is consistent with the fact that, as mentioned above, the probability percentages of the 0_2^+ S, P, and D components are almost the same as those of ^{3}H (^{3}He) as shown in Table 8.

We remark that this is the first work, with the ab initio calculation, to demonstrate that nuclear clustering is realized in an excited state of multi-nucleon systems by themselves through interactions between them (without the assumption of any clusterization a priori). We note, in Fig. 13 in Sect. 3.2, the same type of clusterization in the dilute excited 0_2^+ states of the ^{4}He-atom tetramer; this property is one of the universal properties in atomic/nuclear systems (see also Fig. 7 in Sect. 3).

In order to examine the drastic change in the spatial structure between the ground and excited states of the four-nucleon system, we calculated [30] the electron inelastic scattering form factors between the states and compared them with the experimental data (see Eqs. (4.1)–(4.4) for definition of the related quantities). Agreement between the observed data and our calculation appears to be quite good (this is the first ab initio four-body calculation to reproduce the data). Therefore, it can be said that the drastic change in the spatial structure between the 0_1^+ to 0_2^+ states is well understood in terms of the GEM four-body calculation.

For a more extensive study, however, a new (e, e') measurement with smaller errors would be required. Such data would contribute significantly to few-body investigations of nuclear spatial excitations.

Finally, we discuss the electric monopole ($E0$) transition and the energy-weighted (EW) $E0$ sum rule for the four-nucleon system. Let $\sum_p r_p^2$ denote the $E0$ operator, r_p being the distance between

Downloaded from https://academic.oup.com/ptep/article/2012/1/01A204/1565231 by University of Manchester user on 22 August 2022

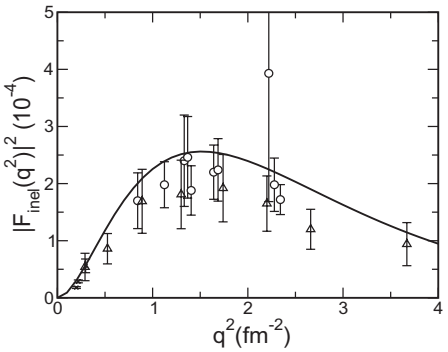

Fig. 18. Form factor for the inelastic electron scattering ^{4}He$(e, e')^4$He(0_2^+) by the four-body calculation (solid line) [30] and the available data. Taken from Ref. [30].

a proton and the c.m. of ^{4}He, and the sum running over protons. In the case where the interactions commute with the $E0$ operator, the sum rule can be written as

$$\sum_{n\geq 2}^{\infty}(E_n - E_1)|\langle 0_n^+|\sum_p r_p^2|0_1^+\rangle|^2 = \frac{\hbar^2 Z}{m_N}\langle r_p^2\rangle_{0_1^+}, \tag{4.9}$$

where E_n and $|0_n^+\rangle$ are the energy and wave function of the nth state of the four-nucleon system, respectively, m_N being the nucleon mass, and $Z = 2$. Completeness is assumed for the set of states $\{|0_n^+\rangle; n = 1, \ldots, \infty\}$, which are normalized in a sufficiently large volume.

The calculated and observed $E0$ matrix elements are $1.38\,\mathrm{fm}^{-2}$ and $1.10 \pm 0.16\,\mathrm{fm}^{-2}$, respectively. The contribution from the second 0^+ state to the LHS value of Eq. (4.9), the sum rule limit, is only 11% experimentally [61,62] and 17% theoretically. The second 0^+ state is not a collective mode. The contribution of some 200 pseudo-continuum states, which are nonresonant discretized continuum states, obtained by diagonalizing the Hamiltonian, above the 0_2^+ state below $E_\mathrm{x} = 60\,\mathrm{MeV}$ amounts to 70% of the LHS value. Thus, we understand that a major part of the EW $E0$ sum rule is exhausted by nonresonant, low-energy continuum states.

The AV8′ potential does not strictly commute with the $E0$ operator. Therefore, Eq. (4.9) does not strictly hold; in our model space, summation in LHS saturates at $E_\mathrm{x} \sim 300\,\mathrm{MeV}$ with some 3 000 pseudo-continuum states and exceeds the RHS value by 4%. However, we verified that, for the Minnesota NN force [63] which does commute with the $E0$ operator, the LHS value of Eq. (4.9) exhausts 99.9% of the RHS value with $\langle r_p^2\rangle_{0_1^+}$ calculated using the force. This means that our four-body 0^+ basis functions form an approximately complete set in our finite space and, therefore, are reliable in the investigation of the 0^+ states and the (e, e') form factor.

In this way, we have succeeded in showing that the four-body calculation using realistic NN forces plus a phenomenological NNN force can explain the drastic change of the spatial structure in going from the ground state to the second 0^+ state in ^{4}He.

5. Application to hypernuclear physics

In this section, we show examples of the GEM study of hypernuclear structure. There are many interesting and important subjects that can be addressed by solving the Schrödinger equations for four-body and five-body systems.

One of the primary goals of hypernuclear physics is to extract information on baryon–baryon interactions. By making use of the YN scattering data and the complementary NN data, several

Downloaded from https://academic.oup.com/ptep/article/2012/1/01A204/1565231 by University of Manchester user on 22 August 2022

types of YN one-boson-exchange (OBE) potential models have been proposed within the $SU(3)$ and $SU(6)$ frameworks. However, such YN and YY OBE models exhibit a great deal of ambiguity at present, since YN scattering experiments are extremely limited and there are no YY scattering data. Therefore, it is important to obtain information on YN and YY interactions from hypernuclear structure studies following a strategy, illustrated in Fig. 3, that combines few-body calculation and spectroscopy experiments. Successful examples of such studies are discussed in our review papers [37–40] on hypernuclear physics.

In this section, as typical examples, we review the structure of ${}^{4}_{\Lambda}$H, ${}^{4}_{\Lambda}$He, and the double Λ hypernucleus, ${}^{11}_{\Lambda\Lambda}$Be.

5.1. *The first four-body calculation of* ${}^{4}_{\Lambda}$H *and* ${}^{4}_{\Lambda}$He*, and* Λ–Σ *conversion*

Four-body calculation of ${}^{4}_{\Lambda}$H and ${}^{4}_{\Lambda}$He using realistic NN and YN interactions is much more difficult than that of the four-nucleon bound state because one has to take explicit account of the $NNN\Lambda$ and the $NNN\Sigma$ channels as well as the realistic NN and YN interactions (see Ref. [26] for a historical review of this four-body subject).

In Ref. [26], we succeeded in performing full four-body calculations without any restriction of channels. Both the $NNN\Lambda$ and $NNN\Sigma$ channels were incorporated explicitly and all the rearrangement channels of these baryons were taken into account. Later, Nogga et al. [64] performed a more sophisticated four-body coupled calculation using various types of realistic NN and YN potentials, such as Nijmegen models, and they discussed the ΛN–ΣN coupling effect in $A = 4$ hypernuclei. Nemura et al. [65] performed four- and five-body calculations of ${}^{4}_{\Lambda}$H, ${}^{4}_{\Lambda}$He, and ${}^{5}_{\Lambda}$He, taking $\Lambda N - \Sigma N$ coupling and using the same YN potential as in Ref. [43].

In this subsection, we review our GEM study in Ref. [27]; a key issue is how to construct a GEM four-body basis function suitable for the particle conversion interaction. Here, we employ a $\Lambda N - \Sigma N$ coupled YN potential with central, spin-orbit, and tensor terms (S. Shinmura, private communications), which simulates the scattering phase shifts given by NSC97f and is the same YN potential as used in Ref. [43]. The main reason for using this simulated version of NSC97f was that its computational tractability allows us to focus our attention clearly on the physical ingredients. For the NN interaction we employ the AV8′ potential [60]. The observed binding energy of ${}^{3}_{\Lambda}$H is reproduced reasonably: The interaction leads to a Λ binding energy, $B_\Lambda({}^{3}_{\Lambda}\mathrm{H})$, of 0.19 MeV, which agrees well with the observed data ($B_\Lambda({}^{3}_{\Lambda}\mathrm{H} = 0.13 \pm 0.05\,\mathrm{MeV}$).

As for ${}^{4}_{\Lambda}$He and ${}^{4}_{\Lambda}$H, the total four-body wave function is described as a sum of amplitudes for all rearrangement channels of Fig. 19 within the LS coupling scheme:

$$\begin{aligned}\Psi_{JM}({}^{4}_{\Lambda}\mathrm{He},{}^{4}_{\Lambda}\mathrm{H}) = \sum_{Y=\Lambda,\Sigma}\sum_{c=1}^{4}\sum_{\alpha I}\sum_{ss'Stt'} C^{(c)}_{\alpha I ss' Stt'} \\ \times \mathcal{A}\left\{\left[\Phi^{(Y,c)}_{\alpha I}(\mathbf{r}_c,\mathbf{R}_c,\boldsymbol{\rho}_c)\left[[\chi_{s'}(12)\chi_{\frac{1}{2}}(3)]_s\chi_{\frac{1}{2}}(Y)\right]_S\right]_{JM}\right. \\ \left.\times\left[[\eta_{t'}(12)\eta_{\frac{1}{2}}(3)]_t\eta_{t_Y}(Y)\right]_{T=\frac{1}{2}}\right\}, \end{aligned} \tag{5.1}$$

where the spatial basis functions are expressed by

$$\Phi_{\alpha IM}(\mathbf{r},\mathbf{R},\boldsymbol{\rho}) = \left[[\phi_{nl}(\mathbf{r})\psi_{NL}(\mathbf{R})]_K\varphi_{\nu\lambda}(\boldsymbol{\rho})\right]_{IM} \tag{5.2}$$

with a set of quantum numbers $\alpha \equiv \{nl, NL, K, \nu\lambda\}$. Radial parts of the spatial functions, $\phi_{nlm}(\mathbf{r})$, $\psi_{NLM}(\mathbf{R})$ and $\varphi_{\nu\lambda\mu}(\boldsymbol{\rho})$ are described by the Gaussian basis functions, the same as

Downloaded from https://academic.oup.com/ptep/article/2012/1/01A204/1565231 by University of Manchester user on 22 August 2022

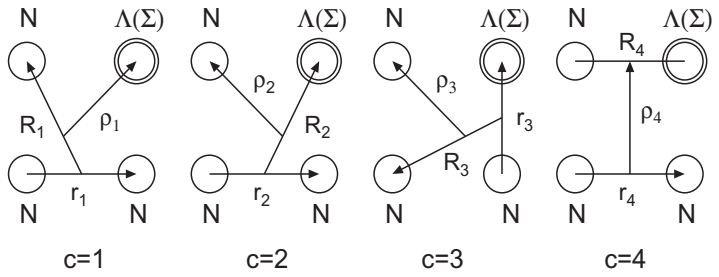

Fig. 19. Jacobi coordinates for the rearrangement channels of the $NNN\Lambda(\Sigma)$ system. The three nucleons are to be antisymmetrized.

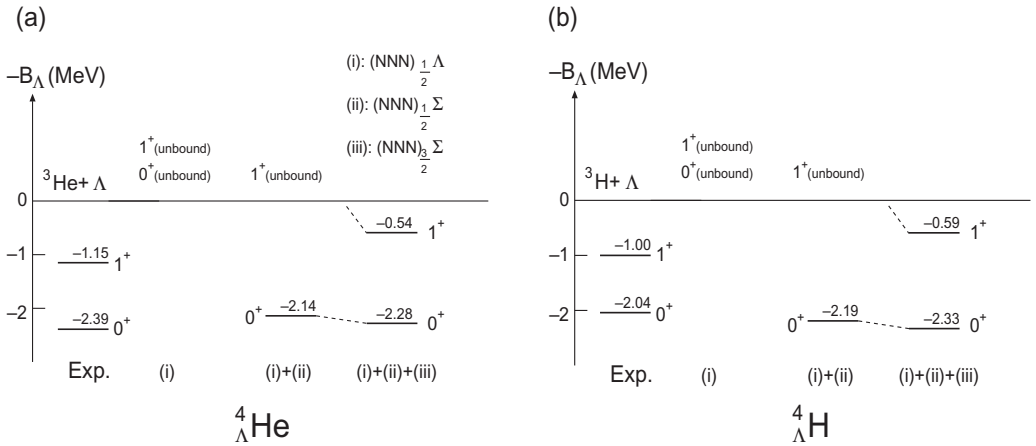

Fig. 20. Calculated energy levels of (a) ${}^{4}_{\Lambda}$He and (b) ${}^{4}_{\Lambda}$H. The channels successively included are (i) $(NNN)_{1/2}\Lambda$, (ii) $(NNN)_{1/2}\Sigma$, and (iii) $(NNN)_{3/2}\Sigma$. The energies are measured from the ${}^{3}\mathrm{He}+\Lambda$ (${}^{3}\mathrm{H}+\Lambda$) threshold. This figure is taken from Ref. [26].

Eqs. (4.4)–(4.6). $\mathcal{A}$ is the three-nucleon antisymmetrizer and χ (η) are the spin (isospin) functions, with the isospin $t_Y = 0(1)$ for $Y = \Lambda(\Sigma)$. Eigenenergies of the Hamiltonian and coefficients C are determined by the Rayleigh–Ritz variational method. The angular momentum space of $l, L, \lambda \leq 2$ is found to be enough to obtain sufficient convergence of the calculated results.

Calculated energies [26] of the 0^+ ground state and the 1^+ excited state of ${}^{4}_{\Lambda}$He and ${}^{4}_{\Lambda}$H are illustrated in Fig. 20 in comparison with the observed values. Here, the $NNN\Sigma$ sector is divided into $(NNN)_{\frac{1}{2}}\Sigma$ and $(NNN)_{\frac{3}{2}}\Sigma$ channels in which three nucleons are coupled to isospin $t = 1/2$ and 3/2, respectively. (i) In the case of taking the $NNN\Lambda$ channel alone, both of the states are unbound. (ii) When the $(NNN)_{\frac{1}{2}}\Sigma$ channel is included, the 0^+ state becomes bound, but the 1^+ state is still unbound. (iii) The 1^+ state becomes bound only when the $(NNN)_{\frac{3}{2}}\Sigma$ channel is switched on. However, the binding energy of the 0^+ state increases only slightly with this $T = 3/2$ channel.

It is found that the Σ-channel components play an essential role in the binding mechanism of the $A = 4$ hypernuclei, the $(NNN)_{\frac{3}{2}}\Sigma$ channel being especially important in the 1^+ state. The calculated binding energy of the 0^+ state almost reproduces the observed binding energy, while the 1^+ state is less bound by 0.6 (0.4) MeV for ${}^{4}_{\Lambda}$H (${}^{4}_{\Lambda}$H), and hence the 0^+–1^+ splitting is larger than the observed splitting. The calculated value of $B_\Lambda({}^{4}_{\Lambda}\mathrm{He}(0^+)) - B_\Lambda({}^{4}_{\Lambda}\mathrm{H}(0^+)) = -0.05$ MeV is different from the experimental one, $+0.35$ MeV, although the Coulomb potentials between charged particles (p, $\Sigma^{\pm}$) are included. This difference should be attributed to the charge-symmetry-breaking

Downloaded from https://academic.oup.com/ptep/article/2012/1/01A204/1565231 by University of Manchester user on 22 August 2022

component, which is not included in our adopted YN interaction (see Ref. [66] for a recent study of the charge-symmetry-breaking effect in ${}^{4}_{\Lambda}$H, ${}^{4}_{\Lambda}$He, ${}^{7}_{\Lambda}$He, ${}^{7}_{\Lambda}$Li($T = 1$), and ${}^{7}_{\Lambda}$Be using an $\alpha NN\Lambda$ four-body model for the $A = 7$ hypernuclei).

The calculated probability percentages of the $NNN\Sigma$-channel admixture are 2.08% and 1.03% for the 0^+ and 1^+ states in ${}^{4}_{\Lambda}$He, respectively. These properties are similar in the case of ${}^{4}_{\Lambda}$H.

In this way, we have developed a calculational method for bound-state problems to make precise four-body calculations of ${}^{4}_{\Lambda}$H and ${}^{4}_{\Lambda}$He, taking both the $NNN\Lambda$ and $NNN\Sigma$ channels explicitly into account and using realistic NN and YN interactions. As a result, we have succeeded in explicating the role of $\Lambda - \Sigma$ conversion and quantitatively estimating the size of Σ mixing in $A = 4$ hypernuclei.

5.2. *Five-body calculation of the double* Λ *hypernucleus* ${}^{11}_{\Lambda\Lambda}$Be *and the Hida event*

In this subsection, we review our recent GEM study [45] of the double Λ hypernucleus ${}^{11}_{\Lambda\Lambda}$Be and the Hida event, taking an $\alpha\alpha n\Lambda\Lambda$ five-body model in which five types of interactions are acting between the three different kinds of particles. The key issues are how to construct the interactions so as to reproduce the binding energies of all the possible subsystems and how to solve the five-body problem with good convergence of the calculated energies.

A double strangeness ($S = -2$) nucleus is an entry to multi-strangeness hadronic systems and requires a unified understanding of YN and YY interactions. The $\Lambda\Lambda$ interaction, in particular, is essential to understand the core of a neutron star, which is expected to include many hyperons. $S = -2$ nuclei will exhibit new dynamical features, which will have more variety than those in ordinary nuclear systems and $S = -1$ ones. The present experimental information on the $S = -2$ system, however, is limited and quite far from such an overview, due to the experimental difficulties of YY scattering in free space as well as producing and hunting for $S = -2$ nuclei.

For this purpose, two important pieces of experimental data obtained by the KEK-E373 experiment have offered a new basis to constrain the $\Lambda\Lambda$ interaction. One is the observation of the double Λ hypernucleus ${}^{6}_{\Lambda\Lambda}$He, which is called the NAGARA event [67]. This event has been uniquely identified on the basis of observing the sequential weak decay, and the experimental $\Lambda\Lambda$ binding (the two-Λ separation energy) was obtained to be $B^{\rm exp}_{\Lambda\Lambda} = 7.25 \pm 0.19^{+0.18}_{-0.11}$ MeV. The other important piece of data in KEK-E373 is the observation of ${}^{10}_{\Lambda\Lambda}$Be, which is called the Demachi–Yanagi event [68,69]. The $\Lambda\Lambda$ binding energy is $B^{\rm exp}_{\Lambda\Lambda} = 12.33^{+0.35}_{-0.21}$ MeV. It was not determined experimentally, however, whether this event was for the ground state or any excited state. We remark that, recently, all the E176/373 emulsion events have been reanalyzed [44] using an updated value for the Ξ^- mass [70] (0.40 MeV larger than the previous one); the newly obtained value for ${}^{6}_{\Lambda\Lambda}$He (NAGARA) is 6.91 ± 0.16 MeV, and that for ${}^{10}_{\Lambda\Lambda}$Be (Demachi–Yanagi) is 11.90 ± 0.13 MeV (see Table I of Ref. [44]). In the present paper, we use these revised values of $B_{\Lambda\Lambda}$.

Recently, the KEK-E373 experiment has reported a newly observed double-Λ event, called the Hida event [44]. This event has two possible interpretations: One is ${}^{11}_{\Lambda\Lambda}$Be with $B_{\Lambda\Lambda} = 20.83 \pm 1.27$ MeV, and the other is ${}^{12}_{\Lambda\Lambda}$Be with $B_{\Lambda\Lambda} = 22.48 \pm 1.21$ MeV (here, the new value for the Ξ^- mass is used). It was also uncertain whether the double-Λ nucleus produced is in the ground state or any excited state. Generally, it is difficult to identify neutral objects such as neutrons and γ ray in emulsion, which leads to serious uncertainties inherent in interpretations of emulsion events. In this sense, the observation of the NAGARA event was epoch-making, being free from this kind of uncertainty. We can consider it as a criterion to give a reasonable interpretation for an emulsion event with several interpretations, for instance, by rejecting those contradictory to the NAGARA data.

Downloaded from https://academic.oup.com/ptep/article/2012/1/01A204/1565231 by University of Manchester user on 22 August 2022

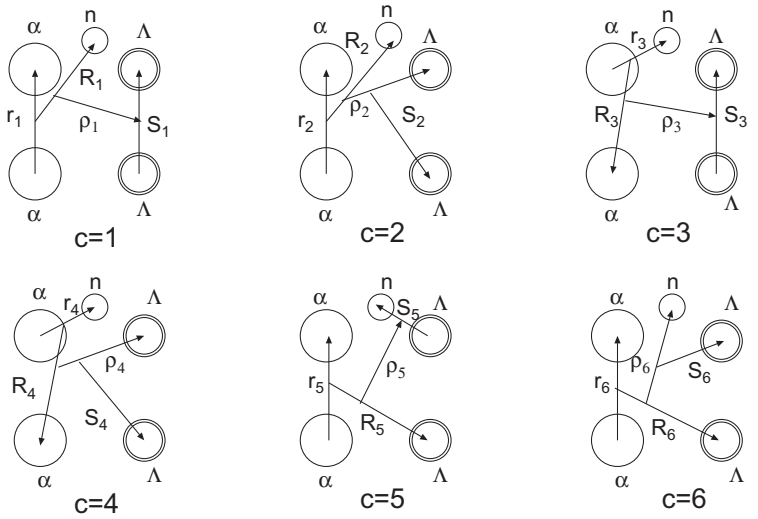

Fig. 21. Example sets ($c = 1$–6) of Jacobi coordinates of the $\alpha\alpha n\Lambda\Lambda$ five-body system. Antisymmetrization (symmetrization) of two Λ (two α) is to be done.

Then, it is vitally important to compare the emulsion data with theoretical analyses to obtain a proper interpretation, where the NAGARA data should be used to choose a reasonable $\Lambda\Lambda$ interaction, as was presented in Fig. 3 for the strategy of hypernuclear study.

For this purpose, we designed, in Ref. [27], the $\Lambda\Lambda$ interaction to reproduce the observed binding energy of ${}^{6}_{\Lambda\Lambda}$He and showed that the Demachi–Yanagi event was interpreted, consistently with the NAGARA event, as the observation of the first excited 2^+ state of ${}^{10}_{\Lambda\Lambda}$Be. We further predicted [27] the energy spectra of p-shell double Λ hypernuclei using the $\alpha x\Lambda\Lambda$ four-body model, where x denoted n, p, d, t, ^{3}He. In this subsection, we show how to interpret the Hida event on the basis of the $\alpha\alpha n\Lambda\Lambda$ five-body calculation for ${}^{11}_{\Lambda\Lambda}$Be.

The $\alpha\alpha n\Lambda\Lambda$ five-body cluster model is quite challenging from the viewpoint of numerical computation, because of the following reasons:

(1) There exist three species of particles (α, Λ, and n).
(2) Five different kinds of interactions (Λ–Λ, Λ–n, Λ–α, α–n, and α–α) are involved.
(3) One must take into account the Pauli principle between the two α particles and between the α and n.
(4) Before going to the five-body calculation, all the interactions are determined so as to reproduce the observed binding energies of the two- and three-body sub-systems ($\alpha\alpha$, αn, $\alpha\alpha n$, $\alpha\Lambda$, $\alpha\alpha\Lambda$, $\alpha\Lambda\Lambda$, and $\alpha n\Lambda$).
(5) Then, the calculated binding energies of the $A = 10$ four-body subsystems, ${}^{10}_{\Lambda}$Be ($= \alpha\alpha n\Lambda$) and ${}^{10}_{\Lambda\Lambda}$Be ($= \alpha\alpha\Lambda\Lambda$), should reproduce the observed values with no additional parameter.

In order to take into account the full five-body degrees of freedom of the $\alpha\alpha n\Lambda\Lambda$ system and the full correlations between all the constituent five particles, we describe the total wave function, $\Psi_{JM}({}^{11}_{\Lambda\Lambda}\mathrm{Be})$, as a function of the *entire* 35 sets of Jacobi coordinates $\{\mathbf{r}_c, \mathbf{R}_c, \boldsymbol{\rho}_c, \mathbf{S}_c; c = 1, \ldots, 35\}$ in which the two Λ (two α) have been antisymmetrized (symmetrized). Some of the important coordinate sets ($c = 1, \ldots, 6$) are shown in Fig. 21.

Downloaded from https://academic.oup.com/ptep/article/2012/1/01A204/1565231 by University of Manchester user on 22 August 2022

The total wave function is described as a sum of five-body basis functions $\Phi^{(c)}_{JM,\beta}$:

$$\Psi_{JM}({}^{11}_{\Lambda\Lambda}\mathrm{Be}) = \sum_{c=1}^{35}\sum_{\beta} C^{(c)}_{\beta}\mathcal{A}_{\Lambda\Lambda}\mathcal{S}_{\alpha\alpha}\,\Phi^{(c)}_{JM,\beta}, \tag{5.3}$$

where $\mathcal{A}_{\Lambda\Lambda}$ ($\mathcal{S}_{\alpha\alpha}$) is the antisymmetrizer (symmetrizer) for two Λ (two α), and

$$\Phi^{(c)}_{JM,\beta} = \xi(\alpha_1)\xi(\alpha_2)\Big[\Big[\Big[[\phi^{(c)}_{nl}(\mathbf{r}_c)\,\psi^{(c)}_{NL}(\mathbf{R}_c)]_I\,\varphi^{(c)}_{n'l'}(\boldsymbol{\rho}_c)\Big]_K\,\Phi^{(c)}_{N'L'}(\mathbf{S}_c)\Big]_L$$
$$\times\Big[[\chi_{\frac{1}{2}}(\Lambda_1)\chi_{\frac{1}{2}}(\Lambda_2)]_\Sigma\,\chi_{\frac{1}{2}}(n)\Big]_S\Big]_{JM}, \tag{5.4}$$

with $\beta \equiv \{nl, NL, n'l', N'L',\ IKL,\ \Sigma S\}$ denoting a set of the quantum numbers. Radial parts of the spatial functions $\phi_{nlm}(\mathbf{r})$, $\psi_{NLM}(\mathbf{R})$, $\varphi_{\nu\lambda\mu}(\boldsymbol{\rho})$, and $\Phi^{(c)}_{N'L'M'}(\mathbf{S})$ are described by Gaussian basis functions, similarly to Eqs. (4.4)–(4.6). In Eq. (5.4), $\xi(\alpha)$ is the internal wave function of an α-cluster with $(0s)^4$ configuration and is used in the folding procedures for the αn, $\alpha\Lambda$, and $\alpha\alpha$ interactions (see Ref. [27] for the treatmen of the Pauli principle between α and α and between α and n). $\chi_{\frac{1}{2}}(\Lambda)$ and $\chi_{\frac{1}{2}}(n)$ are the spin functions of Λ and n, respectively. The expansion coefficients $C^{(c)}_{\beta}$ and the eigenenergy E are obtained by solving the five-body Schrödinger equation using the Rayleigh–Ritz variational method.

We now determine the interactions between subsystems in our $\alpha\alpha n\Lambda\Lambda$ five-body model so that any subsystem composed of two, three, or four constituent particles is reasonably described. In our previous work [27], we determined the α–α, α–n, α–Λ, Λ–n, and Λ–Λ interactions in the $\alpha x\Lambda\Lambda$ four-body cluster model ($x = n$, p, d, t, ^{3}He, and α) for $A = 7 - 10$ systems. These interactions are also employed in the present five-body calculation (see Ref. [45] for a newly added phenomenological $\alpha\alpha n$ three-body potential to properly describe the core nucleus ^{9}Be ($= \alpha\alpha n$), which did not appear in the above model in Ref. [27]).

We remark that the calculated B_Λ value of the ground state (1^-) of ${}^{10}_{\Lambda}$Be, a four-body subsystem, was found to reproduce the observed value well. This successful check of the energies of the subsystems encourages us to perform the full five-body calculation of ${}^{11}_{\Lambda\Lambda}$Be with no adjustable parameter, expecting high reliability for the result. This is a typical procedure for GEM studies of few-body systems.

In Fig. 22, convergence of the calculated energy of the $3/2^-$ ground state of ${}^{11}_{\Lambda\Lambda}$Be is illustrated with increasing number of five-body basis functions $\Phi^{(c)}_{JM,\beta}$ in Eq. (5.3). The energy is measured from the five-body breakup threshold. The lowest threshold is ${}^{10}_{\Lambda\Lambda}\mathrm{Be} + n$, located at -14.68 MeV. The most important configuration in the ground-state wave function is found to be of the $^9\mathrm{Be}^* + \Lambda + \Lambda$ type, namely, the configuration described by using the Jacobi coordinate sets $c = 1, \ldots, 4$ in Fig. 21; here, ^{9}Be* denotes the $\alpha\alpha n$ three-body degrees of freedom.

The additional 4-MeV energy-gain from point (c) to (d) is obtained by including the configurations of the ${}^{9}_{\Lambda}\mathrm{Be}^* + n + \Lambda$ type described with Jacobi coordinates such as $c = 5$ and 6, in which ${}^{9}_{\Lambda}$Be* stands for the $\alpha\alpha\Lambda$ degrees of freedom. Another 1.5-MeV gain from point (d) down to the converged value (-19.81 MeV with an accuracy of 10 keV with a total of $\sim$50 000 basis functions) is achieved by including all the other types of configurations, such as ${}^{10}_{\Lambda\Lambda}\mathrm{Be}^* + n$, ${}^{10}_{\Lambda}\mathrm{Be}^* + \Lambda$, ${}^{7}_{\Lambda\Lambda}\mathrm{He}^* + \alpha$, ${}^{6}_{\Lambda}\mathrm{He}^* + {}^{5}_{\Lambda}\mathrm{He}^*$. Thus, the ground state is found to be bound by 5.1 MeV below the lowest threshold. The angular momentum space of l, l', L, L', $\lambda \leq 2$ was found to be sufficient to obtain convergence for the energy.

Downloaded from https://academic.oup.com/ptep/article/2012/1/01A204/1565231 by University of Manchester user on 22 August 2022

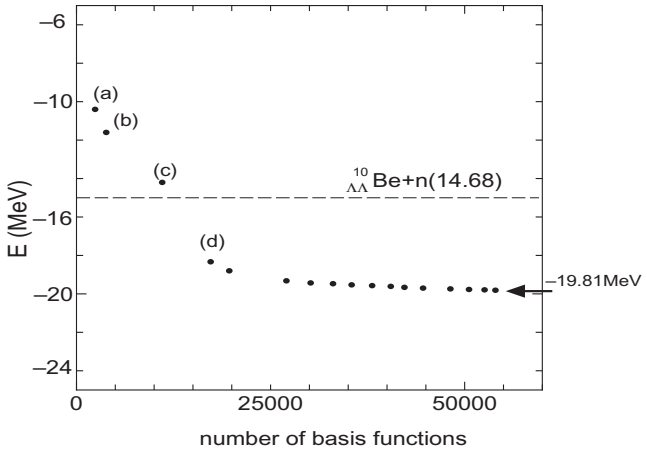

Fig. 22. Convergence of the energy E of the $3/2^-$ ground state in $^{11}_{\Lambda\Lambda}$Be with respect to increasing number of $\alpha\alpha n\Lambda\Lambda$ five-body basis functions. The energy is measured from the five-body breakup threshold. The dashed line shows the lowest $^{10}_{\Lambda\Lambda}$Be $+n$ threshold. Point (a) means the energy obtained taking only a $c = 1$ configuration in Fig. 21, (b) is energy taking $c = 1$ and 2, (c) is obtained by $c = 1$ to 4, (d) is obtained by $c = 1$ to 6. This figure is taken from Ref. [45].

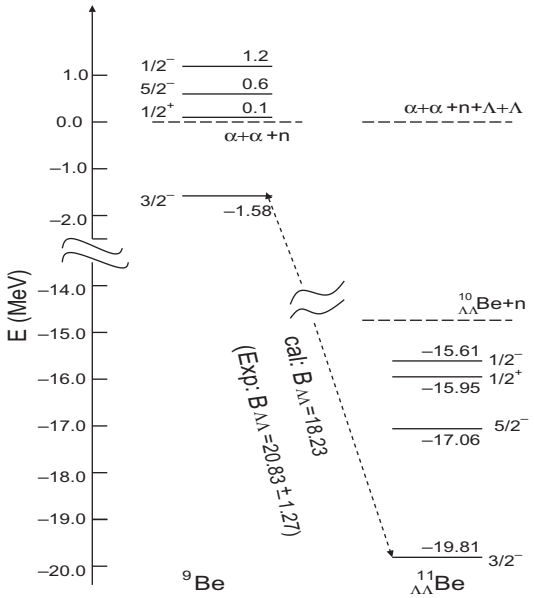

Fig. 23. Calculated energy spectra of the low-lying states of $^{11}_{\Lambda\Lambda}$Be together with those of the core nucleus ^{9}Be. Taken from Ref. [45].

Next, we discuss the energy spectra of $^{11}_{\Lambda\Lambda}$Be and its relation to the Hida event. Using the same framework and interactions as those in the $3/2^-$ ground state, we calculate energies and wave functions of the $5/2^-_1$, $1/2^+_1$, and $1/2^-_1$ states of $^{11}_{\Lambda\Lambda}$Be; there is no other bound state below the lowest $^{10}_{\Lambda\Lambda}$Be $+ n$ threshold. The energy level is illustrated in Fig. 23 together with that of ^{9}Be. Interestingly, the order of the $1/2^+$ and $5/2^-$ states is reversed from ^{9}Be to $^{11}_{\Lambda\Lambda}$Be. This is because the energy gain due to the addition of the Λ-particle(s) is larger in the compactly coupled state $(5/2^-_1)$ than in the loosely coupled state $(1/2^+_1)$ (see Ref. [25] for another example in $^{13}_{\Lambda}$C).

As seen in Fig. 23 the calculated value of $B_{\Lambda\Lambda}(^{11}_{\Lambda\Lambda}\text{Be})$ is 18.23 MeV for the $3/2^-$ ground state, while for the excited states the $B_{\Lambda\Lambda}$ values are calculated to be less than 15.5 MeV. Therefore,

Downloaded from https://academic.oup.com/ptep/article/2012/1/01A204/1565231 by University of Manchester user on 22 August 2022

the observed Hida event can be interpreted as an observation of the ground state of ${}^{11}_{\Lambda\Lambda}$Be. When our calculated binding energy is compared with the experimental value of 20.83 MeV with a large uncertainty of $\sigma = 1.27$ MeV, we can at least say that our result does not contradict the data within 2σ.

For an alternative interpretation of the Hida event as the ground (or any excited) state of ${}^{12}_{\Lambda\Lambda}$Be, a corresponding six-body $\alpha\alpha nn\Lambda\Lambda$ model calculation is necessary, but such an undertaking is beyond our present consideration. Anyway, more precise data are needed to test our present result quantitatively. In the near future, many data for double Λ hypernuclei are expected to be found in the new emulsion experiment E07 at J-PARC. Then, our systematic predictions [27,45] will be clearly tested.

6. Summary

We have reviewed our calculation method, the Gaussian expansion method (GEM) for few-body systems, and its applications to various subjects. These studies have been performed under the strategy illustrated in Fig. 2. Major points to be emphasized are as follows:

i) We introduced three types of basis functions for GEM: Gaussians, complex-range Gaussians, and infinitesimally-shifted Gaussians in which range parameters are chosen to form geometric progression. We demonstrated that the first two types of Gaussian are quite suitable for describing short-range correlations and long-range asymptotic behavior simultaneously and that the second one is also good at describing highly oscillatory wave functions. Use of the third one (mathematically equivalent to the first two) makes the calculation of the Hamiltonian matrix elements quite easy.

ii) Bound-state wave functions of three-body systems are expanded in terms of a set of three-body Gaussian basis functions of the Jacobian coordinates for all three rearrangement channels (similarly for four- and five-body systems). This multi-channel representation makes the functional space much wider than that spanned by single-channel basis functions. Therefore, multi-channel basis functions are particularly suitable for describing both the short-range correlation and weak binding of any pair of particles in the system.

iii) With the use of Gaussian basis functions, calculation of three-, four-, and five-body matrix elements between rearrangement channels can easily be performed for potentials with arbitrary shape. A technique of using the infinitesimally-shifted Gaussian basis functions in place of the Gaussian basis function is very powerful and is used in all the four-body and five-body calculations reviewed in the present paper. The accuracy of the results has been demonstrated, e.g. in a stringent benchmark test calculation [29] for the four-nucleon bound state using a realistic NN interaction.

iv) An advantage of GEM is that the diagonalization of a Hamiltonian using the Gaussian basis functions generates not only the lowest eigenstate but also excited eigenstates with the same J^π simultaneously. To show this advantage, we applied GEM to the very dilute second 0^+ state of a four-nucleon system. We succeeded [30] in describing the second 0^+ state as well as the ground 0^+ state and reproducing ${}^4\mathrm{He}(0^+_1)(e, e'){}^4\mathrm{He}(0^+_2)$ electron scattering data.

v) One of the interesting subject in hypernuclear physics is to investigate the effect of $\Lambda N - \Sigma N$ coupling effect in light Λ hypernuclei. The four-body calculations of ${}^4_\Lambda$H and ${}^4_\Lambda$He taking $\Lambda N - \Sigma N$ coupling explicitly (done for the first time in Ref. [26]) showed the important role of $\Lambda - \Sigma$ conversion, estimating quantitatively the size of Σ mixing in $A = 4$ hypernuclei.

vi) Motivated by the recent observation of the Hida event for a new double Λ hypernucleus, we succeeded in performing a five-body calculation of ${}^{11}_{\Lambda\Lambda}$Be using an $\alpha\alpha n\Lambda\Lambda$ cluster model [45].

Downloaded from https://academic.oup.com/ptep/article/2012/1/01A204/1565231 by University of Manchester user on 22 August 2022

The calculated $\Lambda\Lambda$ binding energy does not contradict the interpretation that the Hida event is an observation of the ground state of ${}^{11}_{\Lambda\Lambda}$Be.

vii) We calculated the ^{4}He trimer and tetramer ground state and excited states using real- and complex-range Gaussians. The states are very weakly bound states under the realistic ^{4}He–^{4}He potential, which has an extremely strong short-range repulsive core; this has made precise calculation difficult. As for the four-body tetramer excited states, we gave, for the first time, a reliable solution in Ref. [34]. We found that precisely the same shape of the short-range correlation as seen in the dimer appears in the trimer and tetramer ground and excited states. By analyzing the accurately obtained asymptotic behavior of the trimer and tetramer excited-state wave functions, we proposed the dimerlike-pair model, which explains intuitively but accurately the dynamics of those very weakly bound few-body systems.

viii) Furthermore, in another study of three- and four-body ^{4}He clusters [35], we found, for the first time, that the six types of correlations between the four binding energies ($B_3^{(1)}$, $B_3^{(2)}$, $B_4^{(1)}$, $B_4^{(2)}$) of the ^{4}He trimer and tetramer ground and excited states (namely, six types of generalized Tjon lines) calculated using 14 kinds of realistic ^{4}He–^{4}He potentials are perfectly linear. In the specific case of the correlation between the ground-state binding energies ($B_3^{(1)}$ and $B_4^{(1)}$), we found a universality that the slope of the atomic Tjon line (4.778) is close to the slope (≈ 5) of the well known nuclear Tjon line in three- and four-nucleon systems. We pointed out, in Fig. 7, another universality between atomic and nuclear systems: that the level structure of ground and excited states of the ^{4}He dimer, trimer, and tetramer is quite similar to the $J = 0_1^+$ and 0_2^+ states of ^{8}Be ($=2\alpha$), ^{12}C ($=3\alpha$), and ^{16}O ($=4\alpha$).

Acknowledgements

The author would like to thank Professors M. Kamimura, Y. Yamamoto, T. Motoba, and Th. Rijken for collaboration and discussion. She also thanks Profs. K. Nakazawa and H. Tamura for helpful discussions. The numerical calculations were performed on a HITACHI SR16000 at YITP and KEK.

References

[1] M. Kamimura, Phys. Rev. A **38**, 621 (1988).
[2] M. Kamimura, Muon Catal. Fusion **3**, 335 (1988).
[3] K. Nagamine and M. Kamimura, Adv. Nucl. Phys. **24**, 151 (1998).
[4] M. Kamimura, AIP Conf. Proc. **181**, 330 (1989).
[5] Y. Kino and M. Kamimura, Hyperfine Interactions **82**, 45 (1993).
[6] Y. Kino and M. Kamimura, Hyperfine Interactions **82**, 195 (1993).
[7] Y. Kino, M. R. Harston, I. Shimamura, E.A.G. Armour, and M. Kamimura, Phys. Rev. A **52**, 870 (1995).
[8] H. Kameyama, M. Kamimura, and Y. Fukushima, Phys. Rev. C **40**, 974 (1989).
[9] M. Kamimura and H. Kameyama, Nucl. Phys. A **508**, 17c (1990).
[10] E. Hiyama and M. Kamimura, Nucl. Phys. A **588**, 35c (1995).
[11] S. Funada, H. Kameyama, and Y. Sakuragi, Nucl. Phys. A **575**, 93 (1994).
[12] T. Matsumoto, T. Kamizato, K. Ogata, Y. Iseri, E. Hiyama, M. Kamimura, and M. Yahiro, Phys. Rev. C **68**, 064607 (2003).
[13] T. Matsumoto, E. Hiyama, K. Ogata, Y.Iseri, M. Kamimura, S. Chiba, and M. Yahiro, Phys. Rev. C **70**, 061601 (2003).
[14] Y. Kino, M. Kamimura, and H. Kudo, Nucl. Phys. A **631**, 649 (1998).
[15] Y. Kino, M. Kamimura, and H. Kudo, Hyperfine Interactions **119**, 201 (1999).
[16] Y. Kino, M. Kamimura, and H. Kudo, Few-Body Syst. Suppl. **12**, 40 (2000).
[17] Y. Kino, N.Yamanaka, M. Kamimura, P. Froelich, and H. Kudo, Hyperfine Interactions **139**, 179 (2001).
[18] D.E. Groom et al. (Particle Data Group), Eur. Phys. J. C **15**, 1 (2000).

Downloaded from https://academic.oup.com/ptep/article/2012/1/01A204/1565231 by University of Manchester user on 22 August 2022

[19] E. Hiyama, *RCNP Physics Report: RCNP-P-132* (Research Center for Nuclear Physics, Osaka University, Japan, 1994), p. 35.
[20] E. Hiyama: in *Proc. Int. Workshop on the 4-Body Problems, Uppsala, 1995* (Uppsala University, Sweden, 1996), p. 28.
[21] E. Hiyama, Y. Kino, and M. Kamimura, Prog. Part. Nucl. Phys. **51**, 223 (2003).
[22] E. Hiyama, M. Kamimura, T. Motoba, T. Yamada, and Y. Yamamoto, Phys. Rev. C **53**, 2075 (1996).
[23] E. Hiyama, M. Kamimura, T. Motoba, T. Yamada, and Y. Yamamoto, Prog. Theor. Phys. **97**, 881 (1997).
[24] E. Hiyama, M. Kamimura, K. Miyazaki, and T. Motoba, Phys. Rev. C **59**, 2351 (1999).
[25] E. Hiyama, M. Kamimura, T. Motoba, T. Yamada, and Y. Yamamoto, Phys. Rev. Lett. **85**, 270 (2000).
[26] E. Hiyama, M. Kamimura, T. Motoba, T. Yamada, and Y. Yamamoto, Phys. Rev. C **65**, 011301(R) (2001).
[27] E. Hiyama, M. Kamimura, T. Motoba, T. Yamada, and Y. Yamamoto, Phys. Rev. C **66**, 024007 (2002).
[28] E. Hiyama, Y. Yamamoto, T. Motoba, and M. Kamimura, Phys. Rev. C **80**, 054321 (2009).
[29] H. Kamada et al., Phys. Rev. C **64**, 044001 (2001).
[30] E. Hiyama, B.F. Gibson, and M. Kamimura, Phys. Rev. C **70**, 031001 (2004).
[31] Y. Hamahata, E. Hiyama, and M. Kamimura, Hyperfine Interactions **138**, 187 (2001).
[32] E. Hiyama, M. Kamimura, A. Hosaka, H. Toki, and M. Yahiro, Phys. Lett. B **633**, 237 (2006).
[33] M. Kamimura, E. Hiyama, and Y. Kino, Prog. Theor. Phys. **121**, 1059 (2009).
[34] E. Hiyama and M. Kamimura, Phys. Rev. A **85**, 022502 (2012).
[35] E. Hiyama and M. Kamimura, Phys. Rev. A **85**, 062505 (2012).
[36] P. Naidon, E. Hiyama, and M. Ueda, arXiv:1109.5807 [physics.atomic-ph].
[37] E. Hiyama and T. Yamada, Prog. Part. Nucl. Phys. **63**, 339 (2009).
[38] E. Hiyama et al., Prog. Theor. Phys. Suppl. **185**, 106 (2010).
[39] E. Hiyama et al., Prog. Theor. Phys. Suppl. **185**, 152 (2010).
[40] E. Hiyama, Few-Body Syst. **52** (2012), Online First, 14 March 2012.
[41] B. F. Gibson, A. Goldberg, and M. S. Weiss, Phys. Rev. C **6**, 741 (1972).
[42] B. F. Gibson and D. R. Lehman, Phys. Rev. C **37**, 679 (1988).
[43] Y. Akaishi, T. Harada, S. Shinmura, and Khin Swe Myint, Phys. Rev. Lett. **84**, 3539 (2000).
[44] K. Nakazawa and H. Takahashi, Prog. Theor. Phys. Suppl. **185**, 335 (2010).
[45] E. Hiyama, M. Kamimura, Y. Yamamoto, and T. Motoba, Phys. Rev. Lett. **104**, 212502 (2010).
[46] M. Kamimura, Prog. Theor. Phys. Suppl. **62**, 236 (1977).
[47] R.A. Aziz and M.J. Slaman, J. Chem. Phys. **94**, 8047 (1991).
[48] R. Grisenti et al., Phys. Rev. Lett. **85**, 2284 (2000).
[49] V. Efimov, Yad. Fiz. **12**, 1080 (1970) [Sov. J. Nucl. Phys. **12**, 589 (1971)].
[50] V. Efimov, Nucl. Phys. A **210**, 157 (1973).
[51] V. Efimov, Few-Body Syst. **51**, 79 (2011).
[52] E. Braaten and H-W. Hammer, Phys. Rep. **428**, 259 (2006).
[53] E. Braaten and H-W. Hammer, Phys. Rev. A **67**, 042706 (2003).
[54] L. Platter, H.-W. Hammer, and U.-G. Meissner, Phys. Rev. A **70**, 052101 (2004).
[55] R. Lazauskas and J. Carbonell, Phys. Rev. A **73**, 062717 (2006).
[56] G.L. Payne and B.F. Gibson, Few-Body Syst. **14**, 117 (1993).
[57] J.A. Tjon, Phys. Lett. B **56**, 217 (1975).
[58] A. Nogga, S.K. Bogner, and A. Schwenk, Phys. Rev. C **70**, 061002 (2004).
[59] L. Platter, H.-W. Hammer, and U.-G. Meissner, Phys. Lett. B **607**, 254 (2005).
[60] B. S. Pudliner, V. R. Pandharipande, J. Carlson, S. C. Pieper, and R. B. Wiringa, Phys. Rev. C **56**, 1720 (1997).
[61] Th. Walcher, Phys. Lett. B, **31**, 442 (1970).
[62] Th. Walcher, Z. Phys. **237**, 368 (1970).
[63] D. R. Thompson, M. LeMere, and Y. C. Tang, Nucl. Phys. A **268**, 53 (1977).
[64] A. Nogga, H. Kamada, and W. Glöckle, Phys. Rev. Lett. **88**, 172501 (2002).
[65] H. Nemura, Y. Akaishi, and Y. Suzuki, Prog. Theor. Phys. **89**, 142504 (2002).
[66] E. Hiyama, Y. Yamamoto, T. Motoba, and M. Kamimura, Phys. Rev. C **80**, 054321 (2009).
[67] H. Takahashi et al., Phys. Rev. Lett. **87**, 212502 (2001).
[68] K. Ahn et al., AIP Conf. Proc. **594**, 180 (2001).
[69] A. Ichikawa, Ph.D. thesis, Kyoto University, 2001.
[70] C. Amsler et al. (Particle Data Group), Phys. Lett. B **667**, 1 (2008).

Downloaded from https://academic.oup.com/ptep/article/2012/1/01A204/1565231 by University of Manchester user on 22 August 2022